



Review

Structural Biology-Based Exploration of Subtype-Selective Agonists for Peroxisome Proliferator-Activated Receptors

Hiroyuki Miyachi

Lead Exploration Unit, Drug Discovery Initiative, The University of Tokyo, 7-3-1 Hongo, Bunkyo-ku, Tokyo 113-0033, Japan; miyachi_hiroyuki@mol.f.u-tokyo.ac.jp

Abstract: Progress in understanding peroxisome proliferator-activated receptor (PPAR) subtypes as nuclear receptors that have pleiotropic effects on biological responses has enabled the exploration of new subtype-selective PPAR ligands. Such ligands are useful chemical biology/pharmacological tools to investigate the functions of PPARs and are also candidate drugs for the treatment of PPAR-mediated diseases, such as metabolic syndrome, inflammation and cancer. This review summarizes our medicinal chemistry research of more than 20 years on the design, synthesis, and pharmacological evaluation of subtype-selective PPAR agonists, which has been based on two working hypotheses, the ligand superfamily concept and the helix 12 (H12) holding induction concept. X-ray crystallographic analyses of our agonists complexed with each PPAR subtype validate our working hypotheses.

Keywords: peroxisome proliferator-activated receptor; PPAR agonist; structural biology; ligand superfamily concept; helix 12 holding induction concept



Citation: Miyachi, H. Structural Biology-Based Exploration of Subtype-Selective Agonists for Peroxisome Proliferator-Activated Receptors. *Int. J. Mol. Sci.* **2021**, *22*, 9223. <https://doi.org/10.3390/ijms22179223>

Academic Editor:
David Arráez-Román

Received: 7 August 2021
Accepted: 23 August 2021
Published: 26 August 2021

Publisher's Note: MDPI stays neutral with regard to jurisdictional claims in published maps and institutional affiliations.



Copyright: © 2021 by the author. Licensee MDPI, Basel, Switzerland. This article is an open access article distributed under the terms and conditions of the Creative Commons Attribution (CC BY) license (<https://creativecommons.org/licenses/by/4.0/>).

1. Nuclear Receptors

Nuclear receptors (NRs) are ligand-dependent transcription factors that modulate diverse aspects of development, reproduction, and energy homeostasis. This receptor superfamily includes receptors for vitamin D, steroid hormones, thyroid hormones and retinoids, as well as a large number of orphan receptors. NRs are composed of six functionally distinct regions (termed A to F) (Figure 1A). The N-terminal AB region is highly variable and contains a constitutionally active transactivation function-1 (AF-1) motif. The central C region (a DNA-binding region) is highly conserved among NRs and contains two zinc finger motifs that make contact with specific nucleotide sequences, termed hormone response elements. The C-terminal D, E and F regions are required for ligand binding and receptor dimerization. In most NRs, these regions also contain a second highly conserved transcriptional activation function-2 (AF-2) motif, which is important for ligand-dependent transcription.

In the basal state, NRs are functionally inactive because they are tightly bound with corepressors, such as NCoR and SMRT. Upon NR binding with an activating ligand, the corepressor dissociates and then coactivators, such as SRC-1 and NCoA, are recruited and the AF-2 helix located in the F region is stabilized to initiate transcription (Figure 1B) [1]. Over the past three decades, much attention has been focused on a subgroup of NRs, the peroxisome proliferator-activated receptors (PPARs).

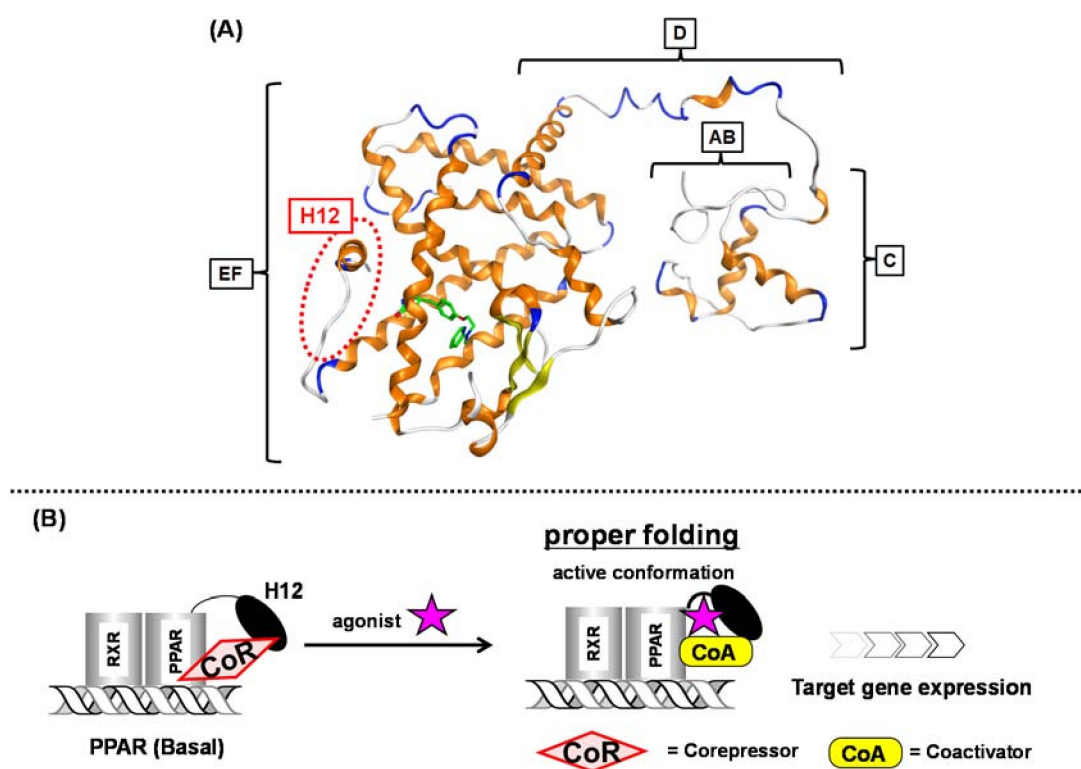


Figure 1. (A) Intact PPAR γ –rosiglitazone complex structure. A to F regions are depicted. The position of H12 (helix 12) is indicated with a red dotted circle. (B) Schematic representation of ligand-dependent nuclear receptor activation (PPAR as an example). PPAR forms a heterodimer with another nuclear receptor, RXR in the nucleus.

2. Peroxisome Proliferator-Activated Receptors

PPARs are activated by endogenous unsaturated and saturated fatty acids and by synthetic ligands [2]. There are three PPAR subtypes: PPAR α , PPAR δ , and PPAR γ . Each PPAR subtype is expressed in a tissue-specific manner. PPAR α is mostly expressed in tissues involved in lipid oxidation, such as liver and kidney. PPAR γ is expressed in adipose tissue, macrophages and vascular smooth muscle, and also in tumors originating from various organs. PPAR δ is expressed in adipose tissue, skeletal muscle, heart, etc. [3].

Upon ligand binding, PPARs heterodimerize with another nuclear receptor, retinoid X receptor (RXR), in the nucleus, and the heterodimers regulate genes expression, such as carnitine palmitoyl acyl-CoA transferase 1A (*CPT1A*), angiopoietin-like protein 4 (*ANGPTL4*) and adipocyte differentiation-related protein (*ADRP*) by binding to specific consensus DNA sequences, termed peroxisome proliferator responsive elements (PPREs) in the promoter regions of target genes. The structural basis of PPREs is a direct repeat of the hexameric AGGTCA recognition motif, separated by one nucleotide (termed DR1) [4].

3. Pleiotropic Effect of PPARs

PPAR subtypes play a key role in lipid, lipoprotein and glucose homeostasis. PPAR α regulates genes involved in fatty acid uptake, β -oxidation, and ω -oxidation. It downregulates apolipoprotein C-III, which regulates triglyceride hydrolysis by lipoprotein lipase, and also regulates genes involved in reverse cholesterol transport, such as apolipoprotein A-I and apolipoprotein A-II [5]. PPAR δ activation regulates HDL cholesterol levels, and it influences glycemic control [6–8]. PPAR δ activation markedly improves glucose tolerance and insulin resistance [9]. PPAR γ is a master regulator of adipocyte differentiation, but recent molecular studies have indicated that its activation is also linked to the expression of many important genes that affect energy metabolism, such as TNF- α , leptin, and

adiponectin [10]. PPAR γ also promotes cell cycle arrest by inhibiting cyclin-dependent kinase activity in several tumor cell lines [11].

Recent extensive biological studies clearly disclosed that PPARs function beyond metabolism. Each PPAR subtype plays major roles in a broad spectrum of biological processes, including cell proliferation and differentiation, fatty acid and eicosanoid signaling, bone formation, tissue repair and remodeling, insulin sensitivity [12].

The above examples demonstrate that PPARs are important pleiotropic NRs and attractive molecular targets for the treatment of various diseases. Therefore, we think it is important to develop potent and PPAR subtype-selective ligands as tools to investigate the detailed functions of individual PPARs. In this review, we summarize in historical order our structural development studies to create PPAR subtype-selective agonists. The discovery of many types of PPAR ligands indicates the validity of our strategy to create subtype-selective NR agonists.

4. Working Hypothesis of the NR Ligand Superfamily

For over twenty years, we have been engaged in NR ligand structure research, which has been based on our working hypothesis of the NR ligand superfamily [13]. The structural and functional features of the many different NRs are similar; therefore, we speculate that all NRs are derived from a single ancestral protein and have structurally evolved to fit various kinds of endogenous NR ligand. Similar evolution of NR ligands would have occurred from an ancestral ligand to form a superfamily of NR ligands, even though they now have diverse structures and functions. Based on this hypothesis, NR ligand structures are divided into two types, basic framework and branch. A common hydrophobic skeleton or a branch that fits into the ligand binding pocket of the basic ancestral protein are characteristic structural motifs that provide NR selectivity. PPAR subtype-selective agonists have certain unique structures associated with subtype selectivity. Examples include, thiazolidine-2,4-dione (TZD) and related structures, exemplified by pioglitazone, for PPAR γ [Figure 2 (1)], the 2,2-dialkyl(usually dimethyl)phenoxyacetic acid structure, exemplified by fenofibrate, for PPAR α [Figure 2 (2)], and the 2,2-unsubstituted phenoxyacetic acid structure, exemplified by GW-501516, for PPAR δ [Figure 2 (3)]. However, based on our working hypothesis, we predict that various kinds of subtype-selective, dual-, and pan-agonists can be created by starting with a common chemical framework as a template.

Based on our hypothesis, we have successfully created various kinds of subtype-selective PPAR agonist, including KCL (PPAR α -selective agonist) [14], APHM-19 (PPAR α -selective agonist) [15], TIPP-401 (PPAR α/δ dual agonist) [16], APHM-13 (fluorescent PPAR α/δ dual agonist) [17], TIPP-204 (PPAR δ -selective agonist) [18], TIPP-703 (PPAR pan agonist) [19], MO-4R (PPAR γ -selective agonist) [20], MEKT-21 (PPAR γ -selective partial agonist) [21], and MEKT-75 (PPAR γ -selective partial agonist) [22]. In addition, in collaboration with Dr. Oyama (Yamanashi University, Japan) and Dr. Shimizu (Tokyo University, Japan), we have solved many X-ray crystallographic structures of PPAR subtypes complexed with our ligands [23–25]. These structural biology studies have been integral to our medicinal chemistry research (Figure 3).

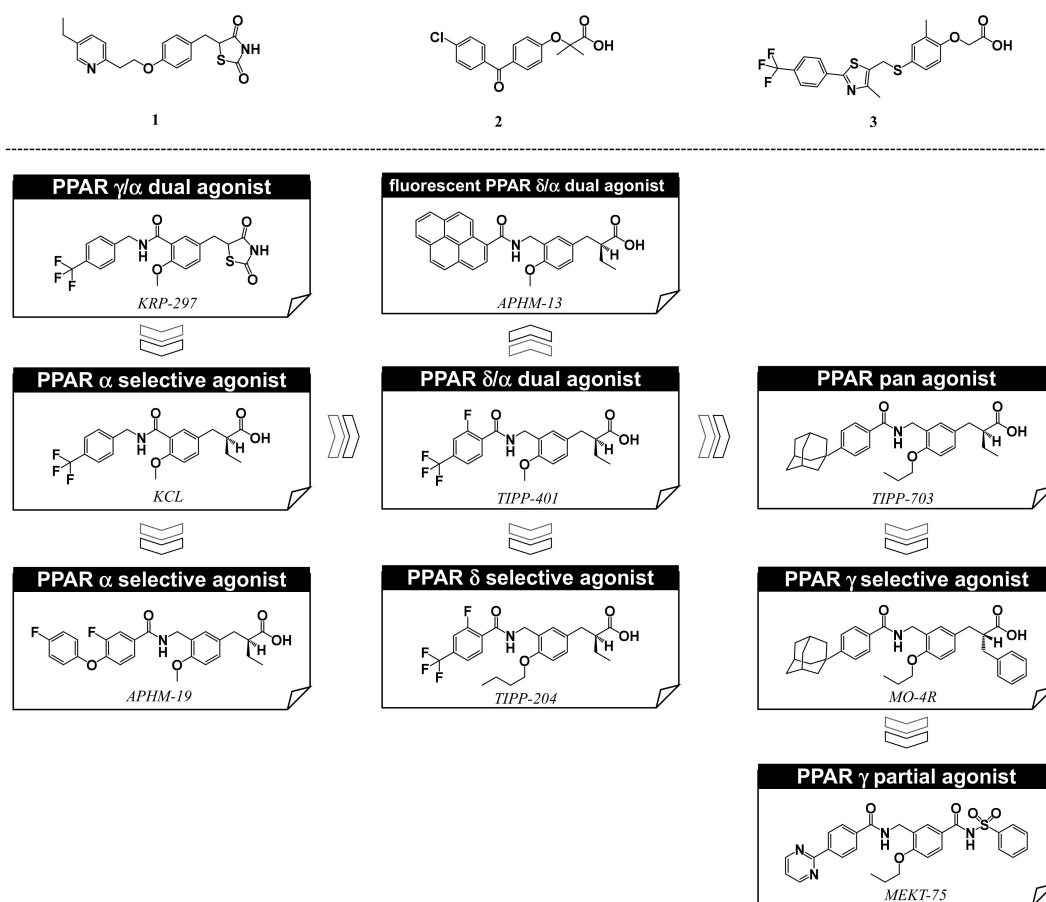


Figure 2. Structures of PPAR γ agonist pioglitazone (1), PPAR α agonist fenofibrate (2), and PPAR δ agonist GW-501516 (3), and, below, our PPAR agonists.

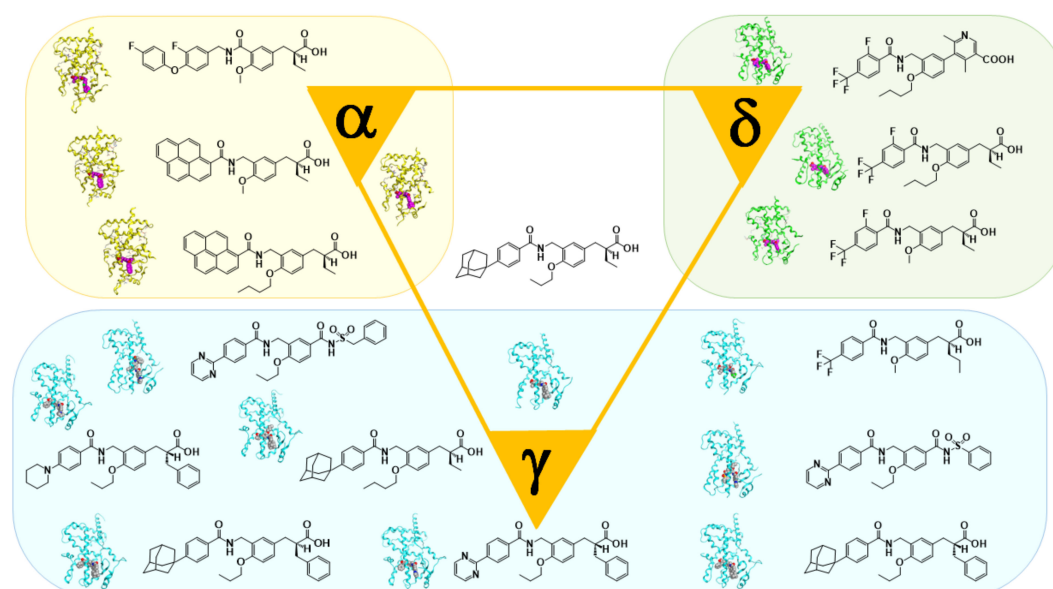
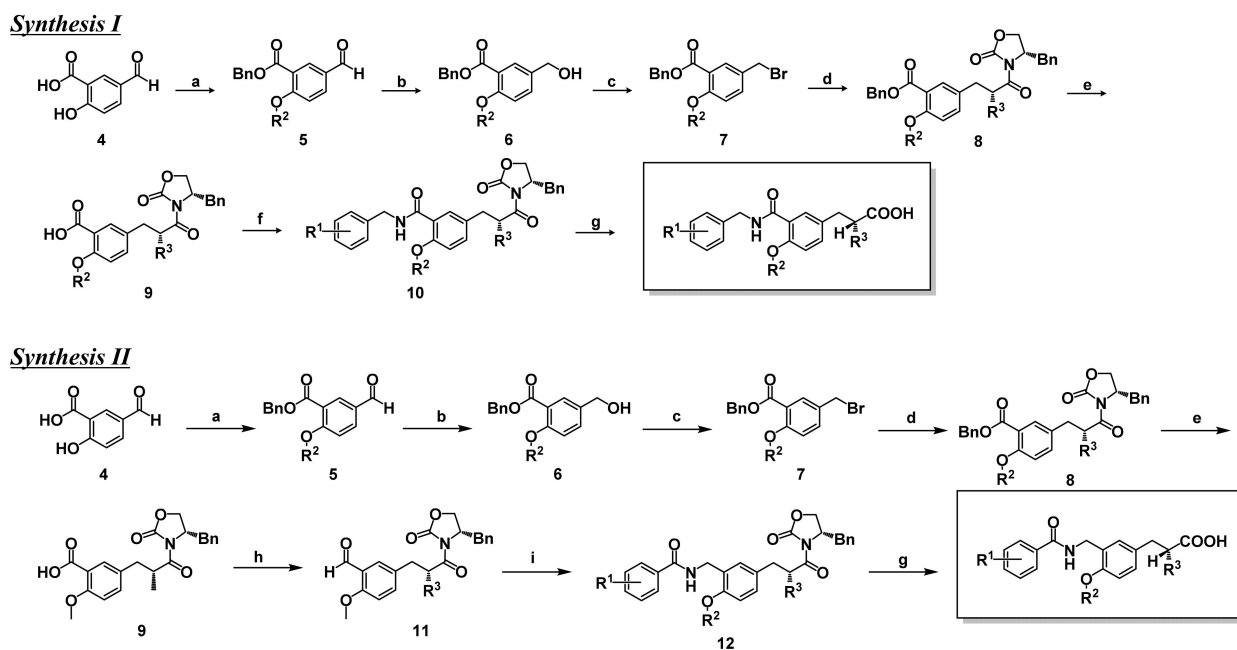


Figure 3. X-ray-crystallographic structures of our representative PPAR agonists complexed with each PPAR ligand binding domain (LBD).

5. Synthesis of Our Ligands

We have designed and synthesized a series of phenylpropanoic acids to develop structurally new PPAR subtype-selective agonists. The agonist synthetic scheme is depicted in Scheme 1. Benzylcarbamoyl-tethering compounds, such as KCL (Figure 2), were prepared by synthesis route I. 5-Formylsalicylic acid (4) was esterified and alkylated to obtain compound 5. The formyl group of 5 was reduced with sodium borohydride (6), then bromination of the hydroxyl group afforded the bromomethyl derivative (7). Evans asymmetric alkylation [26] was performed, followed by hydrogenolysis to afford the key intermediate 9. This was amidated (10), and the chiral auxiliary removed to afford the desired (*S*)-configuration product. The antipodal (*R*) enantiomer was prepared via similar procedures, using (*S*)-*N*-butyryl-4-benzyloxazolidinone as the chiral reagent. Benzamidomethyl-tethering compounds, such as TIPP-401 (Figure 2), were synthesized by synthesis route II. The carboxyl group of key synthetic intermediate 9 was reduced with borane-THF complex, followed by oxidation with activated manganese dioxide to afford the formyl derivative 11. This was amide-alkylated with benzamide derivatives [27], followed by removal of the chiral auxiliary to afford the desired (*S*)-configuration product. The (*R*) enantiomer was also prepared via similar procedures, using (*S*)-*N*-butyryl-4-benzyloxazolidinone as the chiral reagent.



Scheme 1. Synthesis routes of the present series of human PPAR agonists.

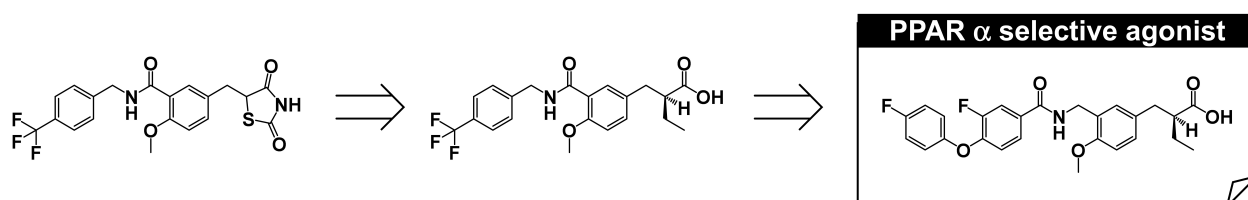
Reagents and conditions:

(Synthesis route I) (a) (1) BnBr, KHCO₃, DMF, rt. (2) R²I, K₂CO₃, DMF, rt. (b) NaBH₄, EtOH, rt. (c) PBr₃, ether, 0 °C. (e) (1) (*R*)-4-benzyl-3-butyryloxazolidin-2-one, LiHMDS, THF, −40–10 °C, (2) benzyl 5-bromomethyl-2-methoxybenzoate, THF, −40–10 °C. (e) H₂, 10% Pd-C, AcOEt, rt. (f) (1) ethyl chloroformate, TEA, THF, −10 °C, (2) R¹-benzylamine, THF, −10 °C–rt. (g) LiOH H₂O, H₂O₂, THF-H₂O, 0 °C.

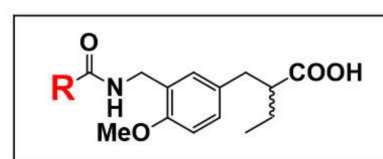
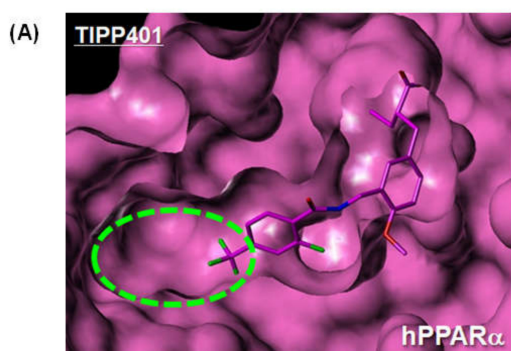
(Synthesis route II) (a) (1) BnBr, KHCO₃, DMF, rt. (2) R₂I, K₂CO₃, DMF, rt. (b) NaBH₄, EtOH, rt. (c) PBr₃, ether, 0 °C. (e) (1) (*R*)-4-benzyl-3-butyryloxazolidin-2-one, LiHMDS, THF, −40–10 °C, (2) benzyl 5-bromomethyl-2-methoxybenzoate, THF, −40–10 °C. (e) H₂, 10% Pd-C, AcOEt, rt. (h) (1) BH₃-tetrahydrofuran, THF, 0 °C. (2) activated MnO₂, CH₂Cl₂, rt. (i) 2-fluoro-4-trifluoromethylbenzamide, triethylsilane, trifluoroacetic acid, toluene, reflux. (g) LiOH H₂O, H₂O₂, THF-H₂O, 0 °C.

6. PPAR α -Selective Agonist: From KCL to APHM-19

In 1996, we started our PPAR ligand discovery program. We aimed to develop PPAR α -selective agonists as anti-dyslipidemic agents by designing and synthesizing a series of substituted phenylpropanoic acid derivatives using as lead compound, KRP-297, a unique TZD derivative with PPAR γ / α dual agonist activity [28–30]. KRP-297 was the first dual active thiazolidinedione (also known as glitazone), a TZD class insulin sensitizer, that binds directly to and activates not only PPAR γ , but also PPAR α with almost equal affinity. Selective PPAR γ activation is a characteristic feature of classical glitazones, including troglitazone, pioglitazone (**1**), and rosiglitazone. We anticipated that replacement of the thiazolidine-2,4-dione ring of KRP-297 with another acidic functionality, such as carboxylic acid, might favor PPAR α selectivity. KRP-297 can be divided into three structural regions: (A) the acidic head, (B) the tether region, and (C) the hydrophobic tail. We performed chemical modification of (A) and (B) and obtained KCL, (S)-2-[4-methoxy-3-(4-trifluoromethylbenzylcarbamoyl)phenylmethyl]butyric acid [14,31–33] as a potent and PPAR α -selective agonist (Figure 4B).



To our surprise, KCL possesses high species-selectivity for transactivation of human PPAR α . KCL activates human, dog, and rat PPAR α with EC₅₀ values of 0.06, 0.16, and 5.2 μ M, respectively. Mutation studies defined specific interaction between the isoleucine at position 272 (Ile272), which is located in the H3 region of the human PPAR α ligand binding domain (LBD), and the hydrophobic tail of KCL [34]. The corresponding amino acid residue in the rat PPAR α LBD is the sterically more bulky phenylalanine. Clinical trials of a KCL-related compound proceeded to phase IIa but were then discontinued.



(B)

R	stereo	EC ₅₀ (nM)			R	stereo	EC ₅₀ (nM)		
		PPAR α	PPAR δ	PPAR γ			PPAR α	PPAR δ	PPAR γ
phenyl	rac	1700 \pm 200	8100 \pm 400	>10,000	4-biphenyl	rac	7.6 \pm 1.9	210 \pm 20	340 \pm 40
4-CF ₃ phenyl	rac	12 \pm 3	110 \pm 12	4400 \pm 400	4-phenethoxyphenyl	rac	60 \pm 13	1400 \pm 100	780 \pm 100
4-phenoxyphenyl	rac	8.8 \pm 0.4	120 \pm 10	820 \pm 140	4F-phenoxyphenyl	S	5.0 \pm 1.3	300 \pm 15	920 \pm 40
3-phenoxyphenyl	rac	41 \pm 4	4800 \pm 700	4600 \pm 500	4Cl-phenoxyphenyl	S	15 \pm 3.0	580 \pm 20	830 \pm 30
2-phenoxyphenyl	rac	3600 \pm 100	>10,000	>10,000	4Br-phenoxyphenyl	S	29 \pm 2.3	800 \pm 30	990 \pm 40
4-benzyloxyphenyl	rac	52 \pm 16	1400 \pm 300	460 \pm 40					

Figure 4. (A) Molecular modeling structure of TIPP-401 bound to the hPPAR α LBD. The binding pocket surrounding the hydrophobic tail is indicated by a light green dotted circle. (B) Transactivation activity of a series of our compounds.

To further strengthen PPAR α agonist activity, we performed a computational docking study to construct binding models of TIPP-401 (a PPAR α / δ dual agonist described later) complexed with the full-length human PPAR α LBD or the human PPAR δ LBD. We noticed that the shapes of the hydrophobic pockets hosting the hydrophobic tail of TIPP-401 (4-trifluoromethyl group) were somewhat different, i.e., the hydrophobic pocket of human PPAR α is wider than that of human PPAR δ (Figure 4A). Therefore, we predicted that if we could introduce a sufficiently bulky substituent instead of the 4-trifluoromethyl group, we would be able to create a more potent human PPAR α -selective agonist, because the introduced substituent would enhance the interaction with the hydrophobic pocket of the human PPAR α LBD. Based on this hypothesis, we discovered a more potent agonist, APHM-19, bearing a bulky 4-fluorophenoxy group in the hydrophobic tail (Figure 4B). We recently solved the X-ray crystallographic structure of APHM-19 complexed with the human PPAR α LBD by the ligand-exchange soaking method [35]. This clearly indicated that the 4-fluorophenoxy group of APHM-19 docks in the hydrophobic pocket composed from Val332, Val255, Leu254, Glu251, Leu247, and Ile241. We also found that the proximal fluorine atom interacted hydrophobically with the side chain of Cys275 (Figure 5C).

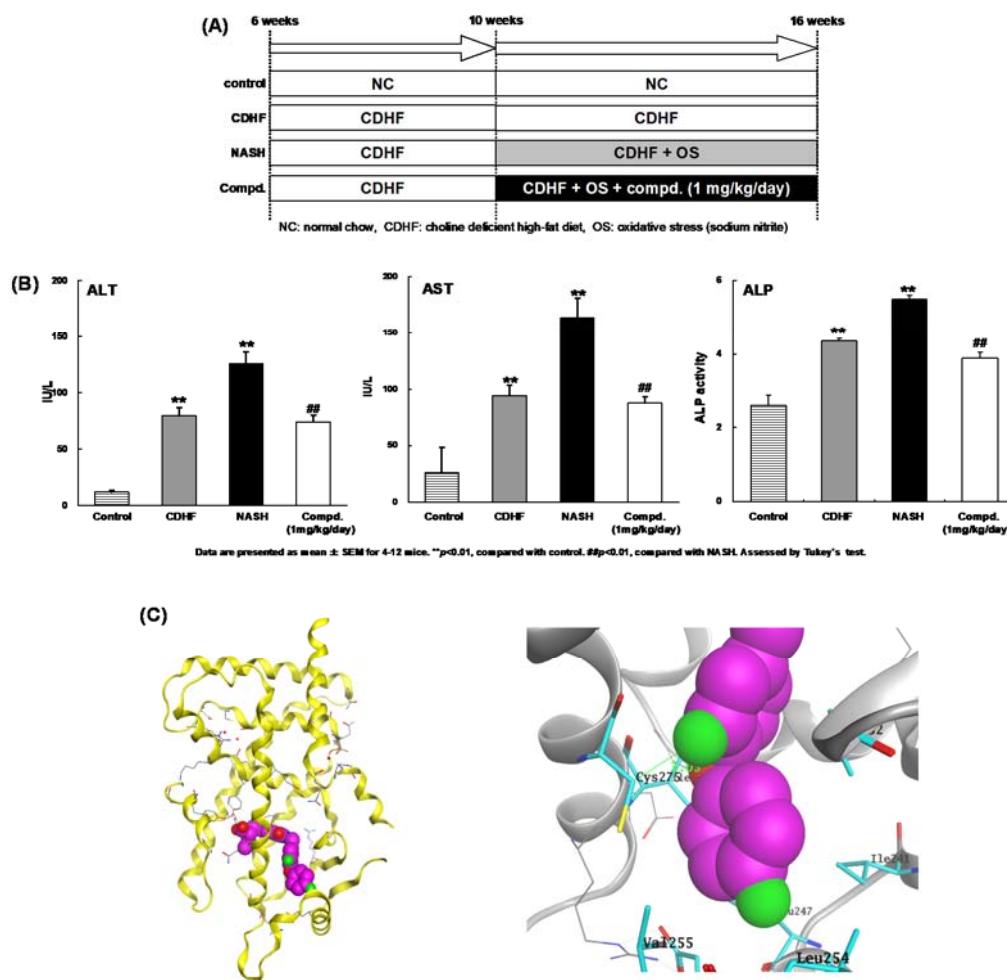
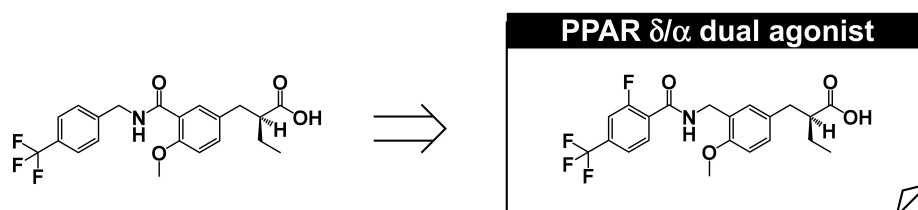


Figure 5. (A) In vivo experiment design. (B) Biochemical markers of hepatobiliary damage. Serum levels of aspartate amino transferase (AST), alanine transaminase (ALT), and alkaline phosphatase (ALP) in the four experimental groups were measured at the end of the study period. Each value represents the mean \pm SEM of five rats. ## $p < 0.01$ versus normal control group, ** $p < 0.01$ versus choline-deficient high-fat diet fed group (by ANOVA followed by Dunnett's multiple comparison test). (C) (left) Overall crystal structure of APHM-19 complexed with hPPAR LBD. (right) Zoomed view of the hydrophobic tail of APHM-19.

To investigate the therapeutic potential of APHM-19, we evaluated its ability to block progression of nonalcoholic steato-hepatitis (NASH) in an animal model [36,37]. Although the pathogenesis of NASH has not been fully elucidated, the “two-hit” theory is widely accepted [38]. The first hit is the accumulation of fatty acids in the liver to cause steatosis. Steatosis causes relatively mild pathology; however, concomitant secondary cellular stress can progress steatosis to steatohepatitis [39,40]. The results are summarized in Figure 5A,B. Aspartate amino transferase (AST), alanine transaminase (ALT), and alkaline phosphatase (ALP) are well-known markers of liver function [41]. Their levels were significantly higher in the NASH rats compared with choline-deficient high-fat diet-fed rats. In the 1 mg/kg/day APHM-19-treated NASH group, liver function was improved compared with the NASH group, although the enzyme levels were still increased compared with normal chow-fed rats. These *in vivo* findings indicate that our PPAR α -selective agonist can block, or at least delay, the progression of NASH. Therefore, PPAR α -selective agonists have therapeutic potential for the treatment of NASH.

7. PPAR α / δ -Dual Agonist: TIPP-401

We next aimed to develop a PPAR α / δ -dual agonist that would effectively activate both PPAR α and PPAR δ subtypes. Pharmacological evidence indicates that PPAR α regulates the expression of genes involved in lipid and lipoprotein homeostasis, while PPAR δ plays a key role in lipid metabolism and insulin resistance. We expected that a compound that effectively activates both PPAR α - and PPAR δ -subtypes might have additive and/or synergistic positive effect(s) in the treatment of metabolic syndrome. We speculated that small manipulations of the KCL structure would affect activities towards both PPAR α and PPAR δ subtypes. We reconsidered the structure–activity relationships of KCL derivatives and noted that a flexible tether has the tendency to decrease PPAR α activation but also to activate PPAR δ . We focused our attention on a hybrid type tether, i.e., –CO–NH–CH₂–, and found that the compound with this tether increased both PPAR α and PPAR δ activity. Slight structural modification at the hydrophobic tail afforded the PPAR α / δ dual agonist, TIPP-401 ((*S*)-2-[3-[(2-fluoro-4-trifluoromethyl-benzoylamino)methyl]-4-methoxybenzyl]butyric acid). A clear enantio-dependency of the transactivation activity of both PPAR subtypes was found. Like KCL, the (*S*) conformer exhibited potent transactivation activity towards both PPAR α and PPAR δ , while the antipodal (*R*) isomer was far less potent.



We succeeded in obtaining the X-ray crystallographic structure of TIPP-401 complexed with human PPAR δ LBD. Hydrogen bonding was observed between the carbonyl oxygen of TIPP-401 and threonine 288 (T288) of PPAR δ (Figure 6), while such hydrogen bonding was not found between the carbonyl oxygen of the KCL-type tether and T288. This might be a reason why the change of tether from amide type to reversed-amide type enhanced the PPAR δ transactivation activity.

As described above, KCL shows species differences for PPAR α . We evaluated the species-selectivity profile of PPAR α transactivation by TIPP-401. As shown in Figure 7A, TIPP-401 activated human and mouse PPAR α with EC₅₀ values of 10 nM, and 1000 nM, respectively. Thus, the transactivation activity of TIPP-401 for PPAR α was approximately 100-fold less in mice than in humans, demonstrating a species preference for humans. We, therefore, performed a mutagenesis study to evaluate the species-selectivity profile of TIPP-401. We found that Ile272 of human PPAR α was also responsible for human-selective PPAR α activation by TIPP-401 (Figure 7B).

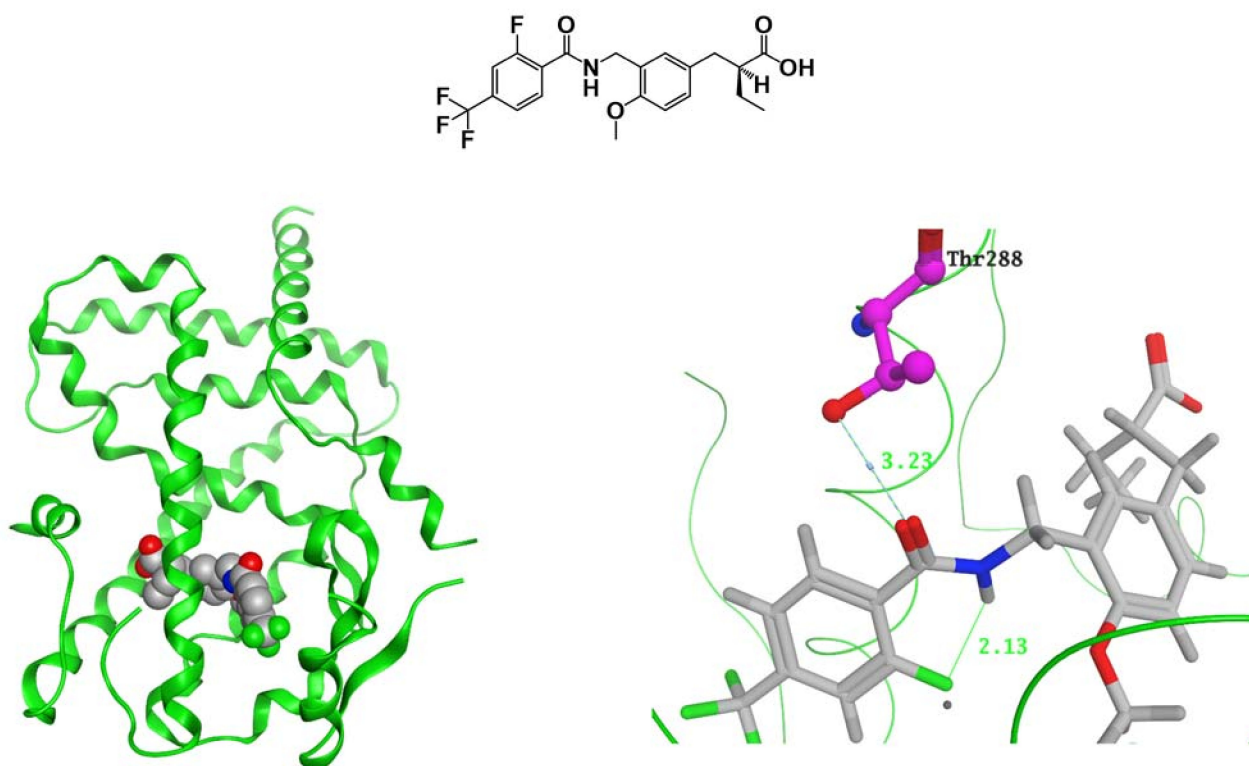


Figure 6. (Left) Crystal structure of TIPP-401 complexed with the PPAR δ LBD. (Right) Zoomed view of the tether region (CONHCH₂) of TIPP-401 hydrogen bonded with 288Thr. Predicted mode of binding of the amide derivative and the reversed-amide derivative to PPAR δ . Hydrogen bonds are shown as yellow dotted lines.

Unfortunately, we have not succeeded in obtaining the X-ray crystallographic structure of TIPP-401 complexed with the human PPAR α LBD. However, the crystal structure of APHM-19 complexed with the human PPAR α LBD, as described above, clearly indicates its importance. The side chain alkyl group of Ile272 hydrophobically interacts with the phenoxyphenyl oxygen of APHM-19 (Figure 7C). Therefore, we speculated that the trifluoromethyl group of TIPP-401 also hydrophobically interacts with the side chain alkyl group of Ile272. In the mouse PPAR α LBD, the corresponding amino acid is phenylalanine. The side chain benzyl group of phenylalanine might be too large to hydrophobically interact with TIPP-401.

TIPP-401 exhibits high nuclear receptor selectivity for PPAR α and PPAR δ because it did not significantly activate Vitamin receptor, PPAR γ , LXR α , RAR α or RXR α at concentrations up to 1 μ M under the experimental conditions used (Figure 8A). To demonstrate the ability of TIPP-401 to activate genes that have PPREs in their promoter regions, we examined changes in expression of representative PPAR-regulated genes in human hepatocellular carcinoma Huh-7 cells. We chose carnitine palmitoyl acyl-CoA transferase 1A (*CPT1A*), angiopoietin-like protein 4 (*ANGPTL4*) and adipocyte differentiation-related protein (*ADRP*) as representative PPAR target genes. These human genes possess PPREs in their promoter regions [42,43]. We investigated the effects of fenofibrate (Feno; a PPAR α -selective agonist), GW-501516 (GW; a PPAR δ -selective agonist) and troglitazone (Tro; a PPAR γ -selective agonist) on transactivation of these genes. The mRNA levels of these genes were augmented subtype selectively by treatment with 50 μ M Feno, 0.1 μ M GW, and 10 μ M Tro (Figure 8B). These results indicated that each PPAR subtype is functionally active in Huh-7 cells. Treatment with 0.1 μ M TIPP-401 augmented *CPT1A* gene expression to an extent comparable with that of obtained with 0.1 μ M GW, and had little effect on *ANGPTL4* expression, probably because of the weak activity of TIPP-401 towards PPAR γ . These results indicate that TIPP-401 is an effective PPAR α/δ dual agonist at the cellular level.

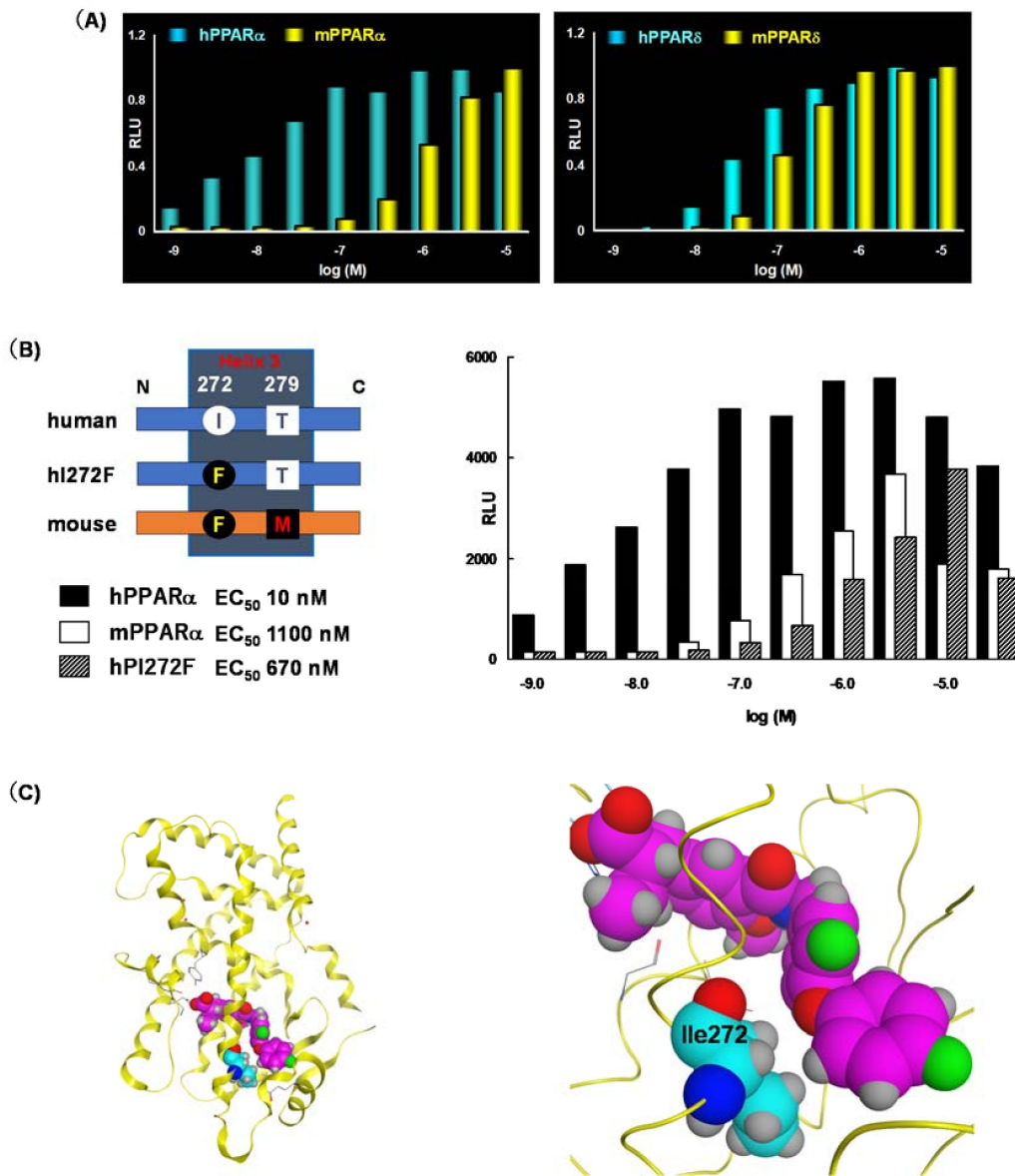


Figure 7. (A) Dose response activation of human and mouse PPAR α and PPAR δ by TIPP-401. (B) Transactivation assay using point mutants of the PPAR α LBD. (C) (left) Overall crystal structure of APHM-19 complexed with PPAR α LBD. (right) Zoomed view of the Ile272 interaction (hydrophobic tail) with APHM-19.

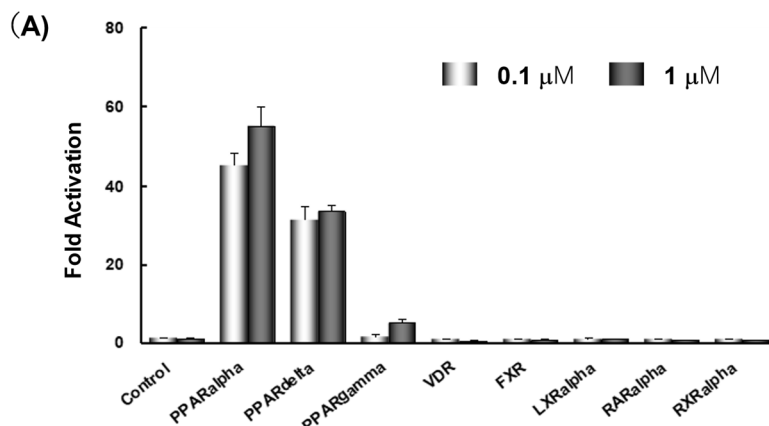


Figure 8. Cont.

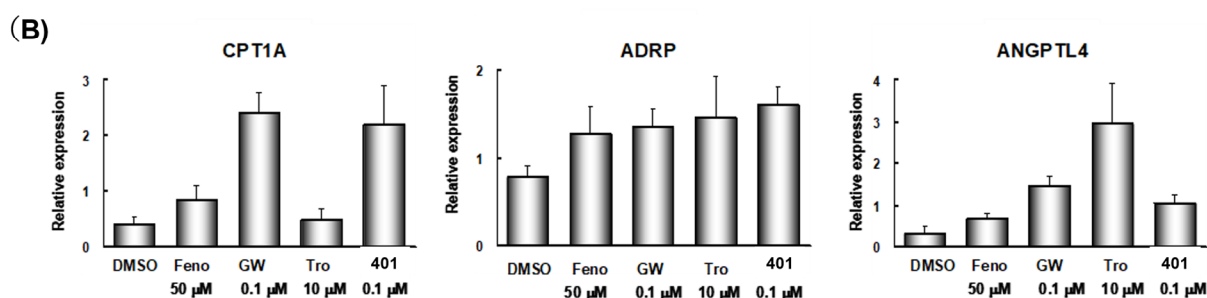
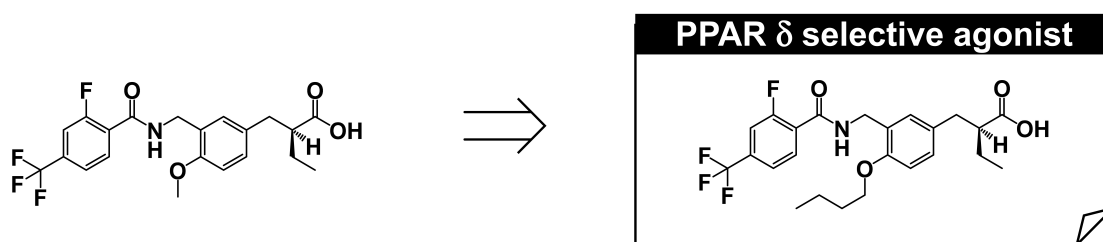


Figure 8. (A) Nuclear receptor cross-reactivity of 0.1 μ M, and 1 μ M TIPP-401. (B) Regulation of expression of representative PPAR-targeted genes by various PPAR ligands.

8. PPAR δ -Selective Agonist: TIPP-204

Our next focus was to create a PPAR δ -selective agonist. Following the description of GW-501516 (3), several PPAR δ -selective agonists have been reported, although most are derivatives of GW-501516, such as (2-methyl)phenoxyacetic acid derivatives [7,44–48]. We aimed to construct phenylpropanoic acid-type PPAR δ -selective agonists, based on the PPAR α/δ dual agonist, TIPP401.



We considered the X-ray crystallographic analysis of PPAR δ complexed with a natural unsaturated fatty acid, eicosapentaenoic acid (EPA) [49]. EPA binds to the cavity in two distinct conformations, i.e., “tail-up” and “tail-down” conformations. The carboxyl group and the first eight carbon units take almost the same configuration in both conformations. However, the distal hydrophobic tail of the tail-up EPA conformer is bent upwards into the upper cavity of the Y-shaped pocket, while in the tail-down conformer, the hydrophobic tail is bent downwards into the bottom cavity of the Y-shaped pocket. Our design was as follows. If we could connect one more sterically bulky hydrophobic side chain to the backbone of TIPP-401, directed towards the upper cavity of PPAR δ , it should have the effect of strengthening PPAR δ activity. We therefore prepared various 3-(4-alkoxyphenyl)propanoic acids, and generated the compound TIPP-204 ((S)-2-[3-[(2-fluoro-4-trifluoromethylbenzoylamino)methyl]-4-butoxybenzyl]butyric acid). We obtained a clear structure–activity relationship confirming that the subtype-selectivity largely depended on the nature of the substituents, as expected (Figure 9A). TIPP-204 exhibited extremely potent PPAR δ transactivation activity, comparable with or even superior to that of the known PPAR δ -selective agonist, GW-501516.

To understand the significance of the *n*-butoxy group introduced at the alkoxy side chain of TIPP-204, we solved the X-ray crystallographic structure of TIPP-204 complexed with the human PPAR δ LBD. We found that the *n*-butoxy group of TIPP-204 is positioned in the small cavity formed by Ile328, Leu303 and Val298. Val298 forms the bottom of the cavity, and Leu303 and Ile328 form the sides of the cavity (Figure 9B). A C4 *n*-butoxy group has the optimal length and further elongation decreases the activity.

Although X-ray crystallography was adequate to identify the key amino acids for human PPAR δ (hPPAR δ) activity, it was not appropriate to investigate the detailed contributions of the three human PPAR δ amino acids to TIPP-204 binding. Reporter assays using a set of GAL4-fusion mutant human PPARs (Figure 10A) indicated that the potent trans-

activation of PPAR δ by TIPP-204 was retained in the L303M mutant, decreased to some extent in the I328M mutant, but greatly decreased in the V298M mutant (approximately 30 times less potent) (Figure 10B). These three mutations all decrease the size of the binding cavity hosting the *n*-butoxy group of TIPP-204, and the rank order of the effect on PPAR δ activity was Val298 > Ile328 > Leu303. In contrast, for GW-501516, the mutant activities showed that the most important amino acid was different from that for TIPP-204. The transactivation of PPAR δ by GW-501516 was retained in the V298M and L303M mutants, but greatly decreased in the I328M mutant (approximately 20 times less potent). Therefore, unlike TIPP-204, Val298 of PPAR δ is less important than Ile328 for PPAR δ selectivity of GW-501516. TIPP-401 showed the same tendency as GW-501516.

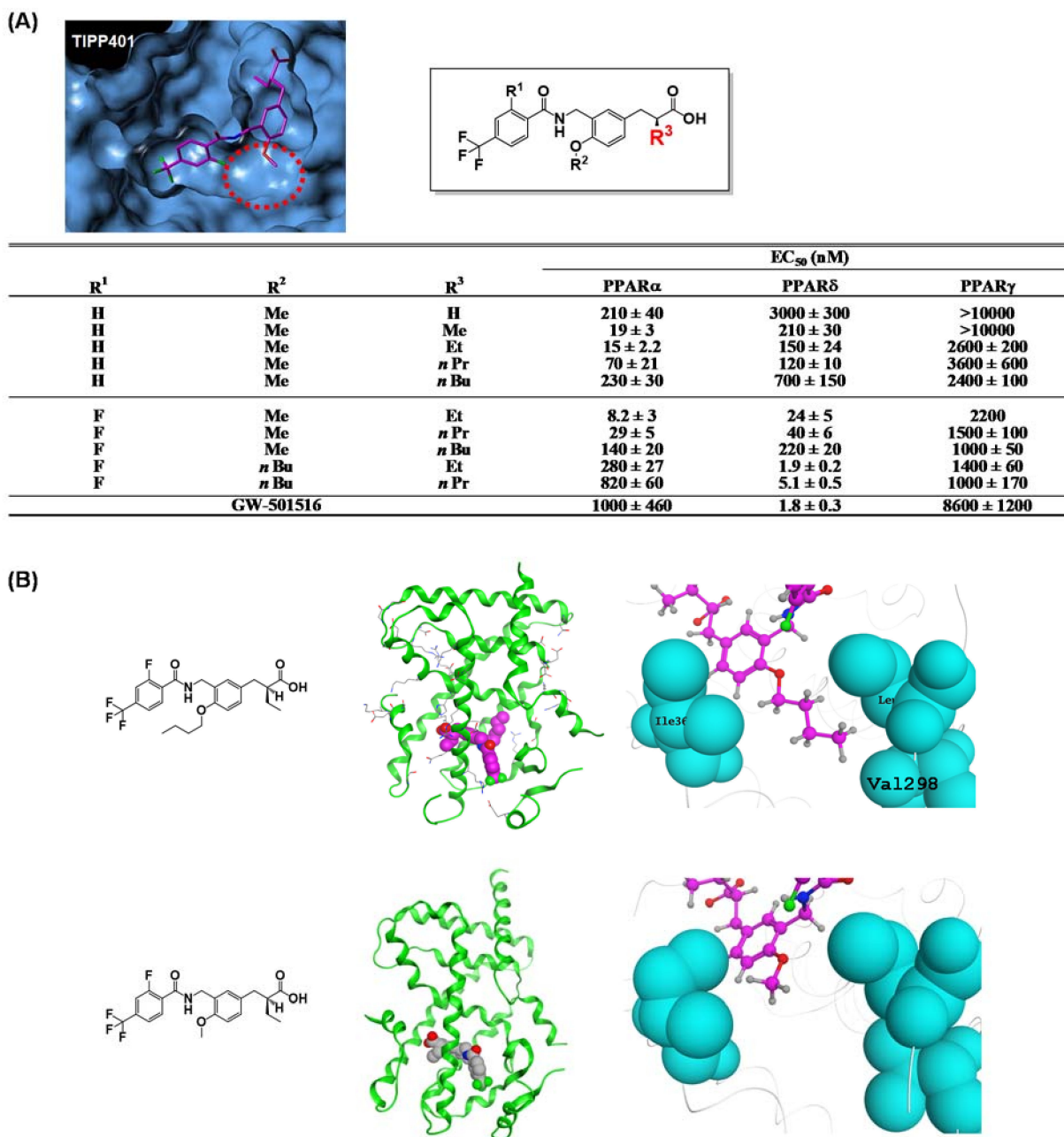


Figure 9. (A) Molecular modeling structure of TIPP-401 bound to the PPAR δ LBD. The binding pocket surrounding the alkoxy side chain is indicated with a red dotted circle. Transactivation activity of a series of compounds is listed in the table. (B) (left) Overall crystal structure of TIPP-401 and TIPP-204 complexed with the PPAR δ LBD. (right) Zoomed view of the alkoxy side chain of TIPP-401 and TIPP-204.

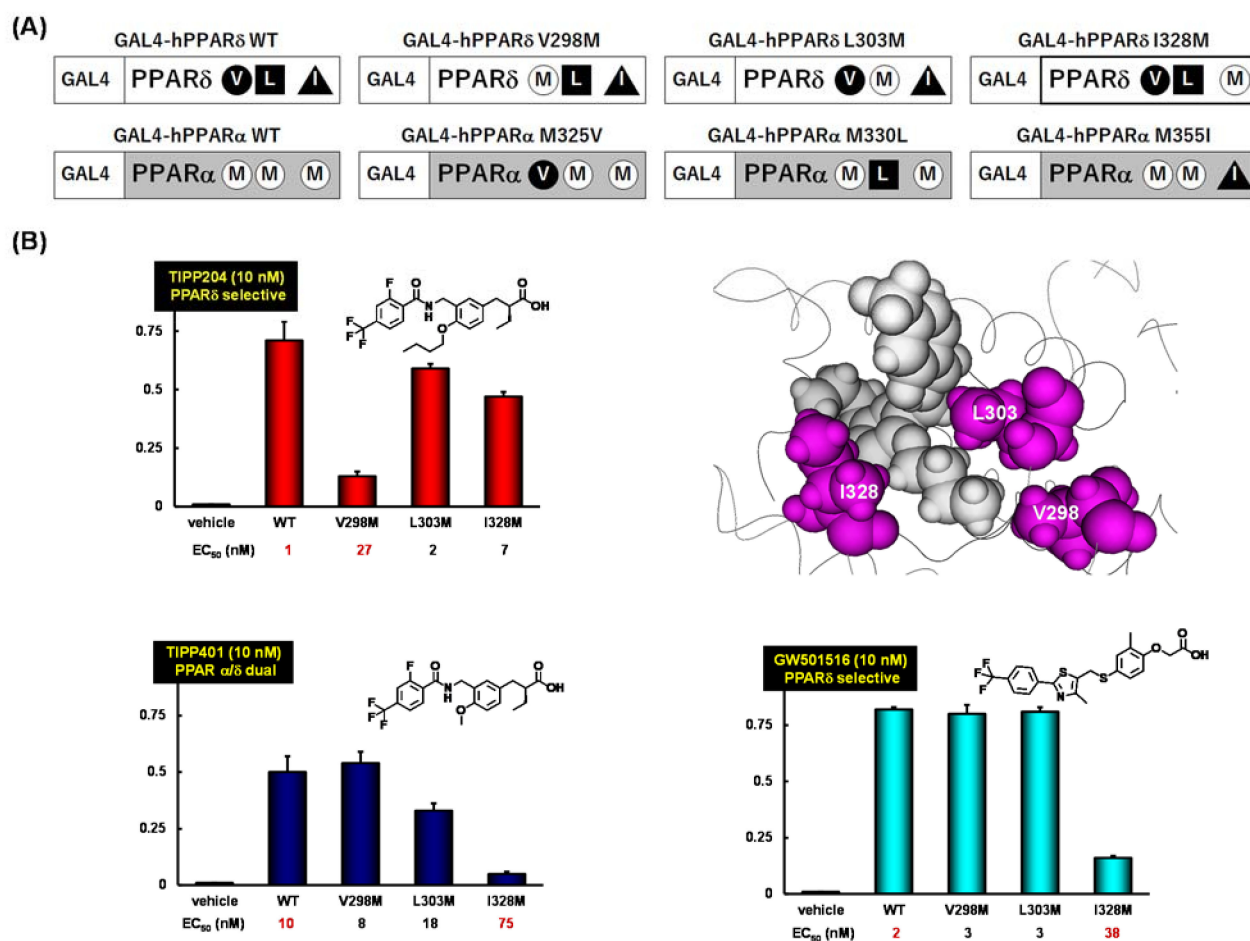


Figure 10. (A) A schematic representation of GAL4-fusion point mutants; (B) Dose responses for transactivation of the GAL4-fusion point mutant constructs with TIPP-204, TIPP-401 and GW-501516.

These mutation studies clearly indicated that the selectivity of human PPAR δ for TIPP-204 is mainly attributed to favorable interactions between the *n*-butoxy group of TIPP-204 and Val298.

9. Fluorescent PPAR α/δ Dual Agonist: APHM-13

We have made extensive use of functional assays in our PPAR agonist discovery research, i.e., transient transactivation assays with CMX-GAL4N-hPPAR LBDs as the recombinant reporter gene. However, affinity-based assays are important because they can determine the direct binding nature of the test compound. Therefore, we designed and synthesized a fluorescent human PPAR α/δ dual-agonist termed APHM-13, which proved suitable for use in homogeneous fluorescence polarization assays [50]. The planar fluorophore pyrene was selected based on the X-ray crystallographic structure of the complex of our human PPAR α/δ dual-agonist, TIPP-401, with the human PPAR α -LBD (Figure 10A,B), in which the distal hydrophobic 2-fluoro-4-trifluoromethylphenyl group of TIPP-401 is located in the cavity of the Y-shaped pocket of the human PPAR α -LBD (Figure 11A). As expected, X-ray crystallography clearly showed that the pyrene ring of APHM-13 was tightly hosted in the hydrophobic cavity (Figure 11C,D). As predicted, the fluorescence intensity of APHM-13 increased with increasing concentration of human PPAR α -LBD in the binding buffer (Figure 11E). However, for human PPAR δ -LBD, APHM-13 exhibited the opposite effect (Figure 11F).

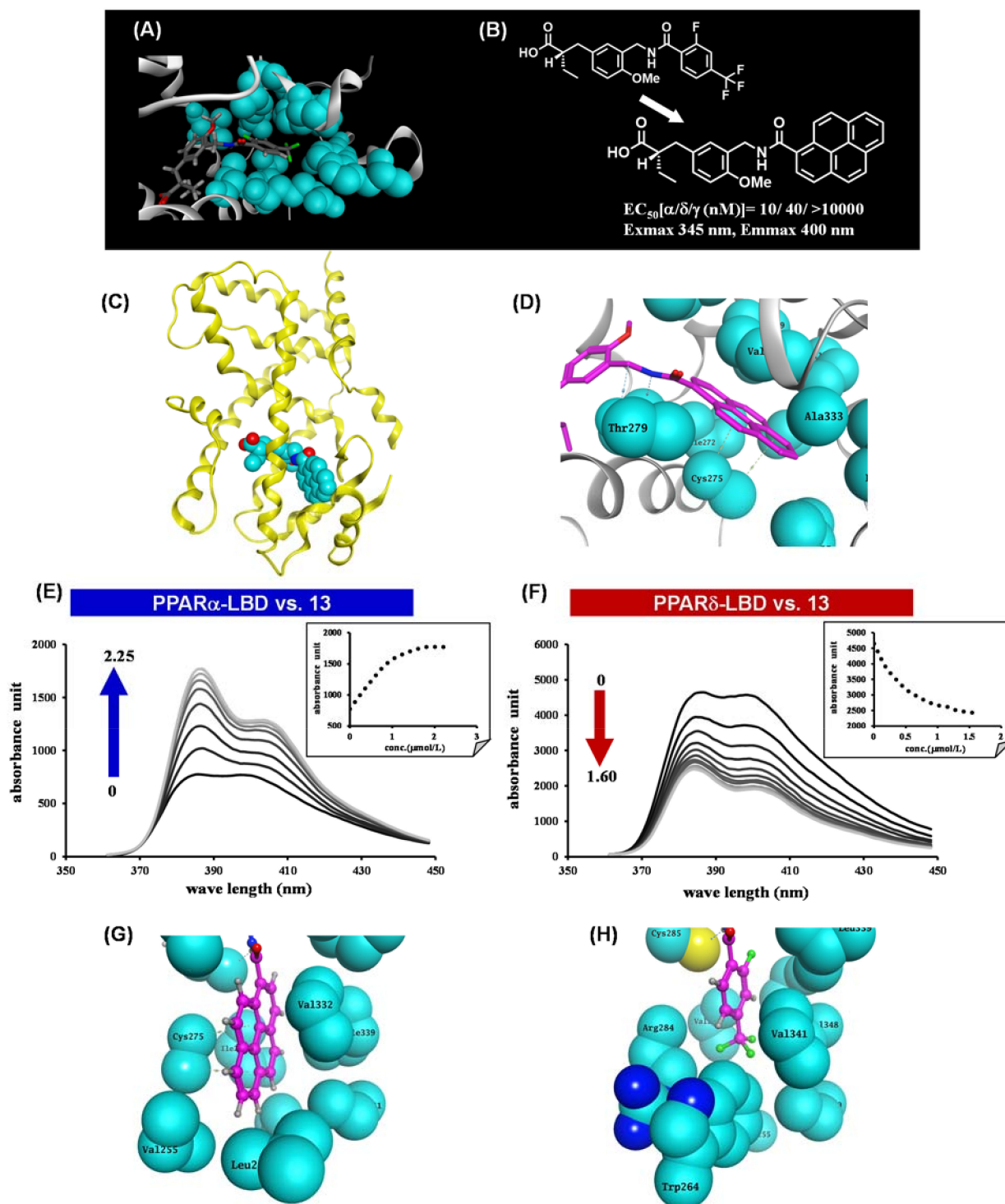
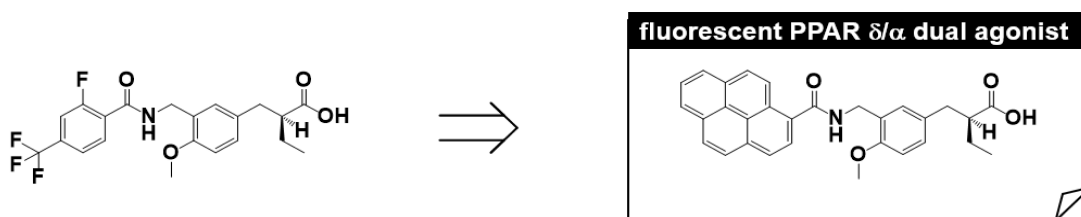


Figure 11. (A) Zoomed view of the hydrophobic tail of TIPP-401 complexed with the human PPAR α LBD. (B) Structural design of APHM-13. (C) X-ray crystallographic structure of APHM-13 complexed with the human PPAR α LBD. (D) Zoomed view of the hydrophobic tail of APHM-13 complexed with the human PPAR α LBD. (E) Fluorescence polarization value changes with the addition of human PPAR α to APHM-13 in PBS. (F) Fluorescence polarization value changes with the addition of human PPAR δ to APHM-13 in PBS. (G) Zoomed view of the hydrophobic interaction of the pyrene ring of APHM-13. (H) Zoomed view of the hydrophobic interaction of the 2-fluoro-4-trifluorophenyl ring of TIPP-401.



These bi-directional fluorescence properties, depending on complexation with either human PPAR α -LBD or human PPAR δ -LBD, were worthy of further exploration. Fluorescence intensity is normally expected to increase upon binding to the target protein because of the hydrophobic nature of the target protein binding pocket. In this context, the increase in fluorescence intensity of APHM-13 upon binding to human PPAR α -LBD is reasonable. There must also be an explanation for the concentration-dependent attenuation of APHM-13 fluorescence upon binding to human PPAR δ -LBD. Figure 11G,H show the binding modes of APHM-13 complexed with human PPAR α -LBD and TIPP-401 complexed with human PPAR δ -LBD, respectively. The pyrene ring of APHM-13 is buried in the Y2 arm of the human PPAR α LBD, which is composed of the side chains of the various hydrophobic amino acids. It is noteworthy that all these amino acids are aliphatic. However, for the human PPAR δ -LBD, the Y2 arm is composed of side chains of Ile249, Leu255, Glu259, Trp264, Val281, Arg284, Val341, Val348, Phe352 and Leu353, i.e., the Y2 arm of the human PPAR δ -LBD contains two aromatic amino acids, Trp264 and Phe352. The trifluoromethyl group of TIPP-401 is less than 2 Å away from Trp264. Therefore, Trp264 might interact with the pyrene moiety of APHM-13 when APHM-13 is bound to the human PPAR δ -LBD.

The naturally occurring aromatic amino acids, tryptophan, tyrosine and phenylalanine, are all intrinsically fluorescent, but tryptophan is the most powerful fluorophore of the three [51]. We speculate that fluorescence quenching involving Trp264 might occur. When APHM-13 in the complex with human PPAR δ -LBD is excited, the obtained fluorescence energy of the excited-state pyrene might be transferred to the nearby Trp264 and attenuated.

To confirm the validity of our hypothesis, we constructed four human PPARs-LBD mutants, i.e., 264Trp of the human PPAR δ -LBD was changed to Leu (hPPAR δ W264L-LBD) and the corresponding Leu of the human PPAR α -LBD was changed to Trp (hPPAR α L258W-LBD), 264Trp of the human PPAR δ -LBD was changed to Ala (hPPAR δ W264A-LBD), and 256Trp of the human PPAR δ -LBD was changed to Ala (hPPAR δ W256A-LBD). We examined the effects of these mutated human PPAR-LBDs on the fluorescence properties of APHM-13. 264Trp but not 256Trp is required for the change of fluorescence properties of APHM-13. The fluorescence of APHM-13 was augmented in the presence of increasing amounts of hPPAR δ W264L-LBD or hPPAR δ W264A-LBD, but not of hPPAR δ W256A-LBD. The fluorescence of APHM-13 was decreased in the presence of increasing amounts of hPPAR δ W225A-LBD (Figure 12B). These results indicated that the critical amino acid associated with the bi-directional fluorescence properties of APHM-13 is residue 264 located in the omega loop position of human PPARs-LBD.

Overall, we created dual-format human PPAR δ and human PPAR α ligand binding assays simply by exploiting fluorometric changes elicited by the binding of endogenous and/or exogenous ligands.

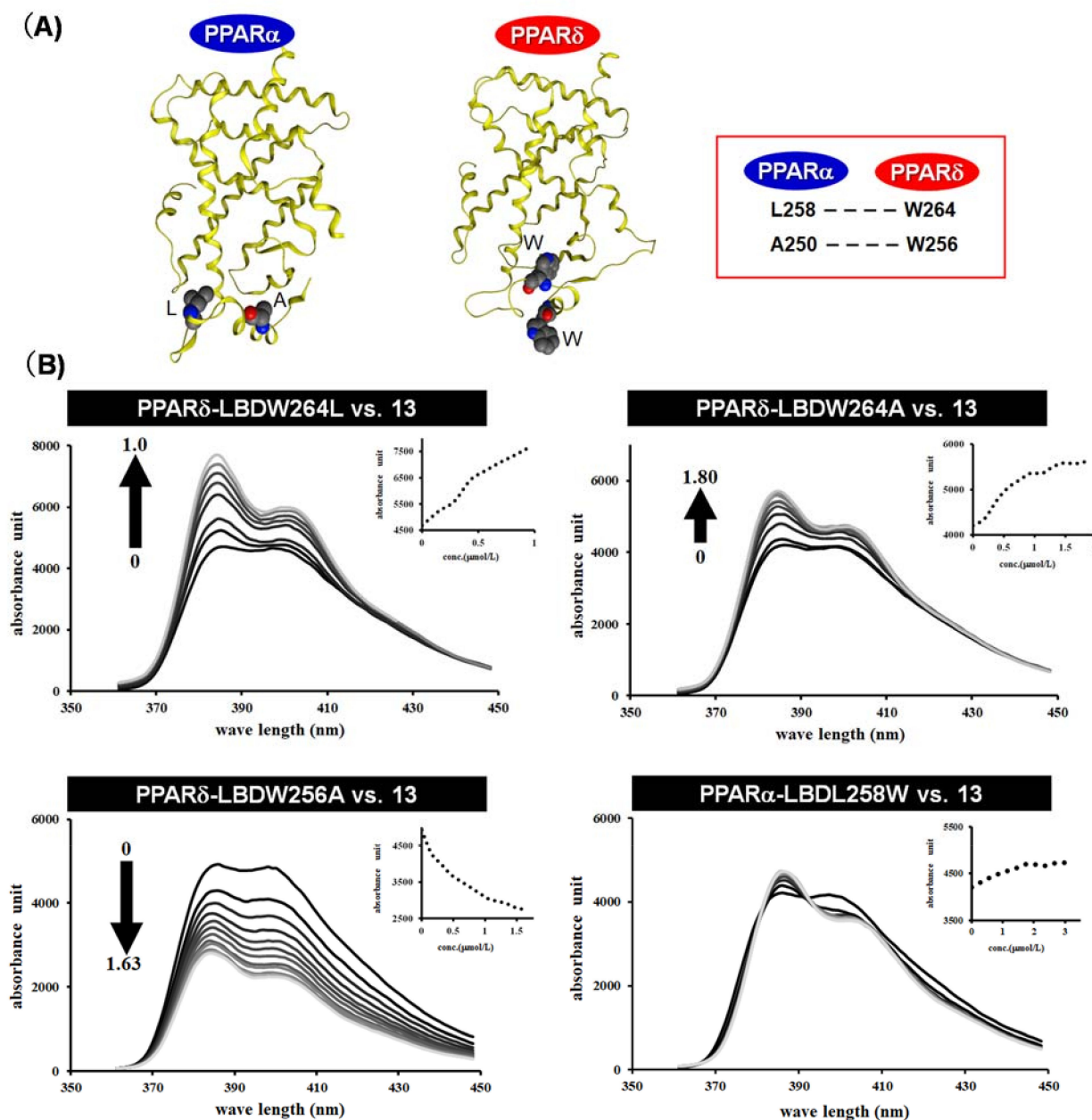


Figure 12. (A) X-ray crystallographic structure of the human PPAR α LBD and human PPAR δ LBD. Important amino acids hosting the pyrene moiety are indicated. (B) Fluorescence polarization value changes with the addition of mutated human PPAR to APHM-13 in PBS.

10. PPAR Pan Agonist: TIPP-703

We have shown that the structure of 3,4-disubstituted phenyl propanoic acid is a good PPAR pharmacophore, especially for PPAR α and PPAR δ . However, we consider that this framework is not suitable for PPAR γ . We therefore aimed to create a 3,4-disubstituted phenyl propanoic acid PPAR agonist, preferentially with PPAR γ agonistic activity. To achieve this, we reassessed the three-dimensional structural differences among PPAR LBDs, especially the hydrophobic binding pocket hosting the hydrophobic tail of our PPAR agonists. We noticed that the two pairs of amino acids that interpose the substituent attached at the 4-position of the distal benzene ring of our agonists were different. These were Arg and Trp for PPAR δ , Cys and Leu for PPAR α , and Gly and Leu for PPAR γ (Figure 13A). We believed that the PPAR γ LBD possesses the widest binding pocket for hosting the 4-position of the substituent. Therefore, we designed and synthesized

compounds with a bulky substituent at the 4-position (Figure 13B) and found an adamantyl group (TIPP-703) to be preferable (Figure 13C).

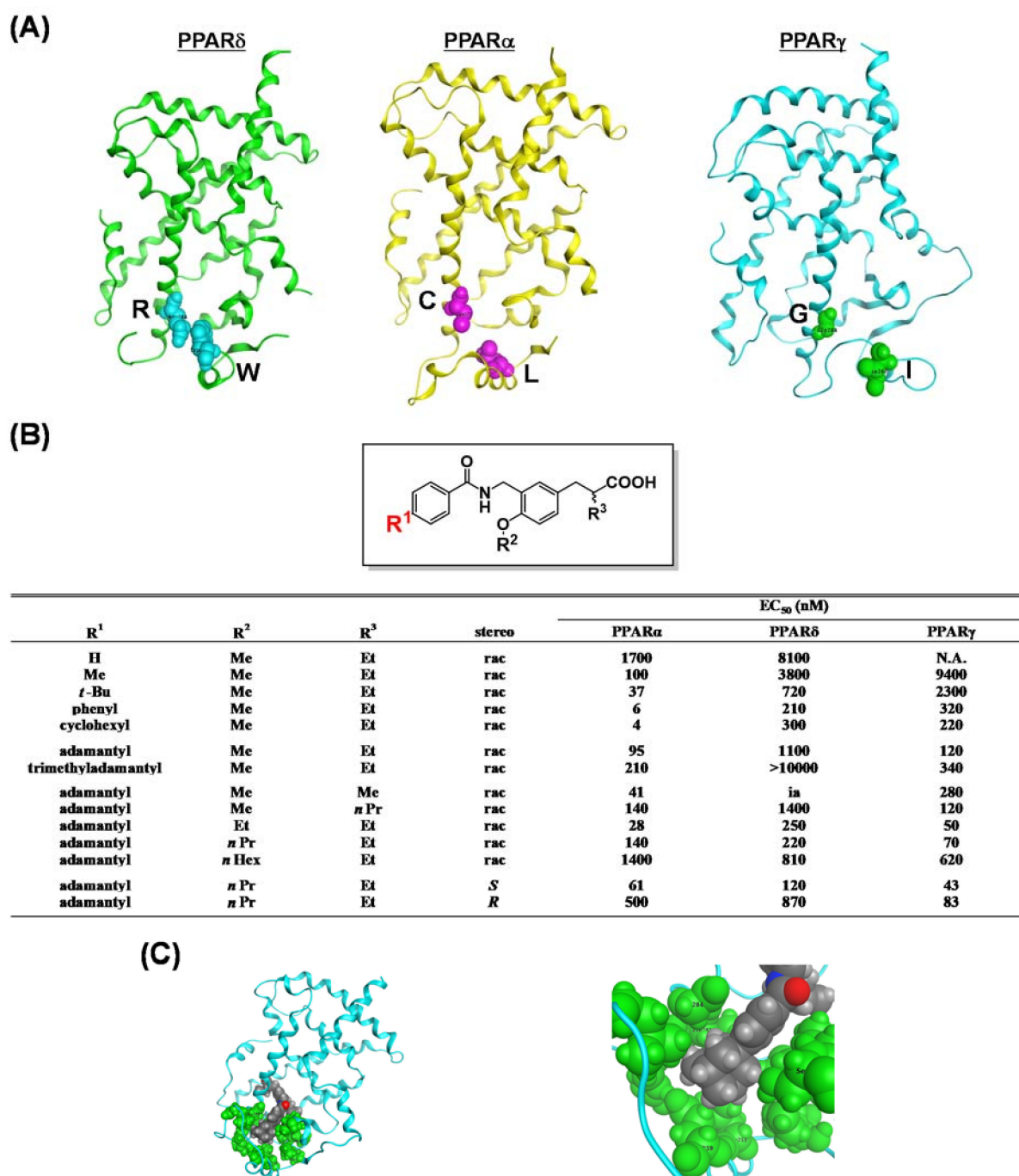
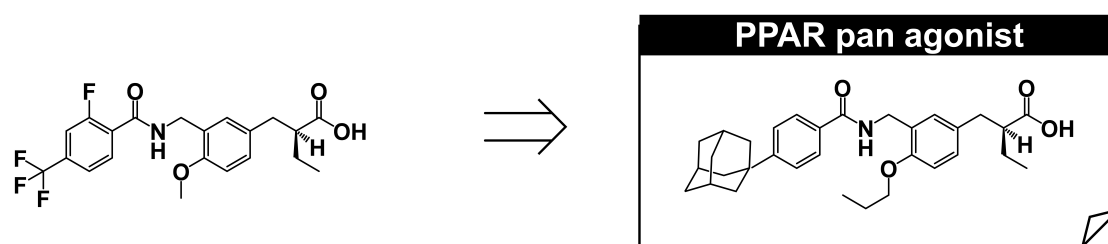


Figure 13. (A) Crystal structures of hPPAR δ , hPPAR α and hPPAR γ LBDs. (B) PPAR agonist activities of a series of compounds. (C) (left) Structure of the whole hPPAR γ LBD–TIPP-703 complex. (right) Zoomed view of the amino acids that interact with the hydrophobic tail of TIPP-703 complexed with the hPPAR γ LBD. The side chain amino acids and the ligand are depicted with space-filling models.



TIPP-703 is a PPAR pan agonist (EC_{50} values of all three PPAR subtypes are approximately 100 nM or less in our assay system) that can simultaneously activate all PPAR subtypes. Considering the beneficial pharmacological effects of each PPAR subtype, a PPAR pan agonist is extremely attractive, especially for the treatment of metabolic syndrome, stroke, heart failure, sudden cardiac death, and certain cancers [52]. Simultaneous activation of all PPARs might also reduce the occurrence of adverse side effects, such as weight gain, fluid accumulation, and pulmonary and macular edemas, which are often associated with PPAR γ agonists, such as rosiglitazone and pioglitazone [7].

We compared the ability of MCC-555 [53], rosiglitazone (PPAR γ agonists), and TIPP-703 to stimulate adipocyte differentiation of murine preadipocyte 3T3-L1 cells (Figure 14B). PPAR γ agonists promote the conversion of a variety of preadipocyte and stem cell lines into mature adipocytes [54]. All three compounds dose-dependently stimulated adipocyte differentiation and induced triglyceride accumulation. The ability of TIPP-703 to differentiate preadipocytes is similar to that of rosiglitazone, and far more potent than that of MCC-555.

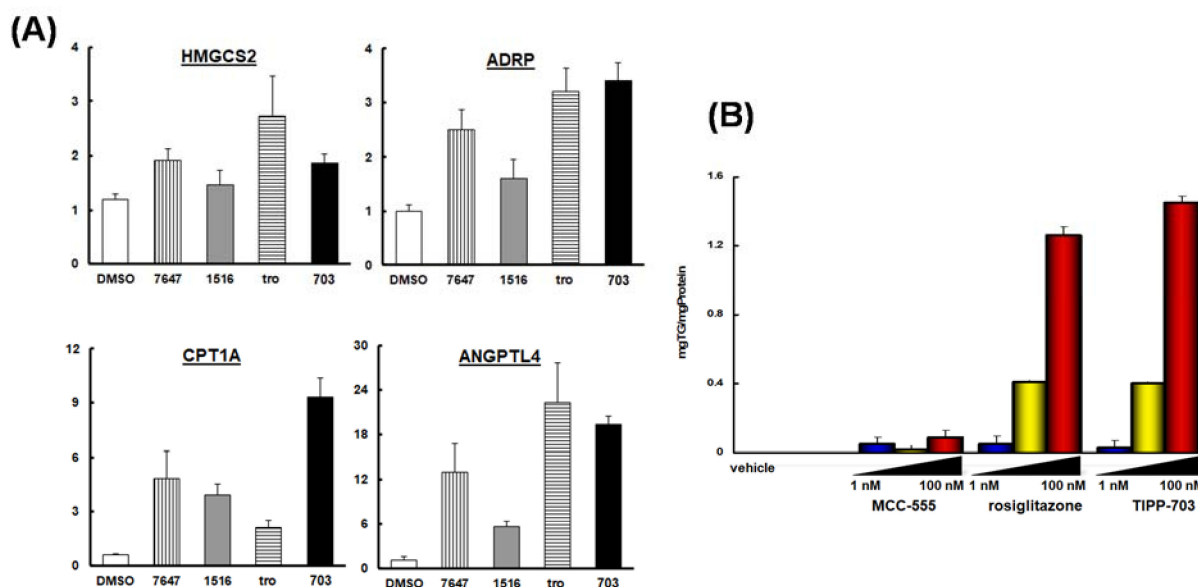


Figure 14. (A) Changes in the expression of selected genes (*CPT1A*, *HMGCS2*, *ADRP* and *ANGPTL4*) in Huh-7 cells in response to several PPARs agonists. (B) Induction of adipocyte differentiation by PPAR agonists, MCC-555, rosiglitazone, and TIPP-703.

To further characterize TIPP-703 as a PPAR pan agonist, we assessed its effects on representative genes having a PPRE in the promoter region in human hepatocellular carcinoma Huh-7 cells (Figure 14A). Carnitine palmitoyl acyl-CoA transferase 1A (*CPT1A*), HMG-CoA synthase 2 (*HMGCS2*), adipocyte differentiation-related protein (*ADRP*) and angiopoietin-like protein 4 (*ANGPTL4*) were selected, as human genes that possess a PPRE in the promoter region [55,56].

Treatment with TIPP-703 augmented the expression of all four genes, to a similar extent to that obtained with the positive control agents. These results indicate that TIPP-703 is an effective PPAR pan agonist and can activate various kinds of PPAR-regulated genes

at the cellular level. We also evaluated the effect of TIPP-703 as an anti-pancreatic cancer agent. Expression of PPAR γ was confirmed in two pancreatic cell lines, PANC-1 and PT-45 (Figure 15A). When PT-45 cells were treated with 1 μ M TIPP-703, induction of G1 phase arrest was observed (Figure 15B). Biochemical studies indicated that TIPP-703 treatment enhanced expression of the cyclin-dependent kinase inhibitor, p21 (Cip1/Waf1) [57], and caused subsequent attenuation of cyclin D1 expression in both PANC-1 and PT-45 cells. p27 expression was not affected by TIPP-703 treatment (Figure 15C) [58]. These results provide strong evidence that activation of PPARs is a promising mechanism for the treatment of pancreatic cancer. Further in vivo experiments are ongoing.

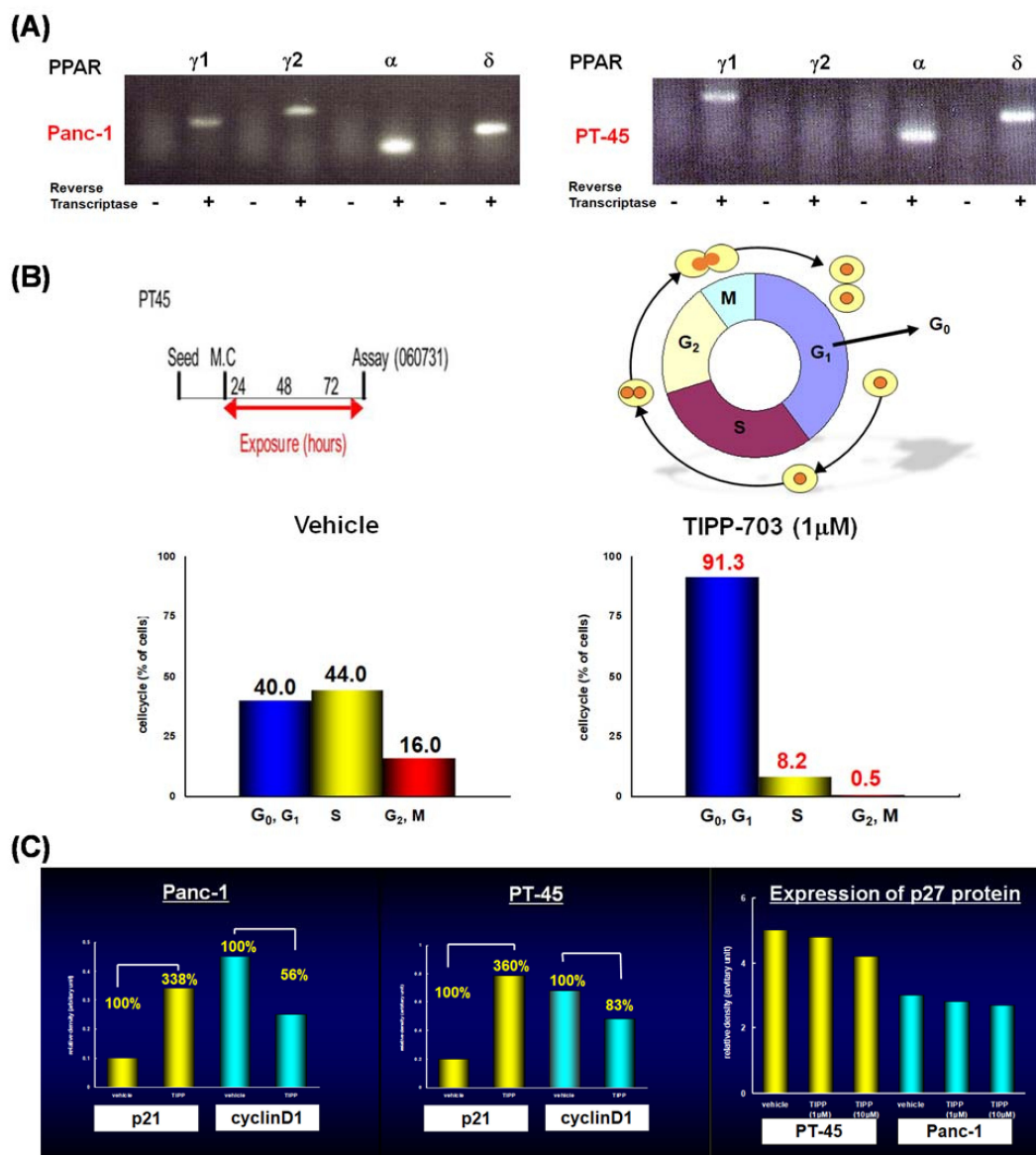


Figure 15. (A) Expression of PPAR subtypes in PANC-1, and PT-45 cells. (B) Effect of TIPP-703 on the cell cycle of PT-45 cells. (C) Effect of TIPP-703 on the expression of P21, cyclinD1, and p27 in both PANC-1 and PT-45 cells.

11. PPAR γ -Selective Agonist: MO-4R

We next aimed to improve PPAR γ selectivity and to create a PPAR γ -selective agonist using a phenyl propanoic acid framework. We reviewed the three-dimensional structural differences among PPAR LBDs, focusing on the binding pocket hosting the side chain alkyl group of the acidic propanoic acid moiety. We noticed the difference in the two aromatic amino acids in the PPAR γ and PPAR α LBDs, which are positioned at the pocket entrance

of the side chain alkyl group of the propanoic acid moiety. For PPAR γ this was His and for PPAR α the bulkier Tyr (Figure 16A). We also focused the different aliphatic amino acids in PPAR γ and PPAR δ LBDs, positioned at the bottom of the cavity hosting the side chain alkyl group. For PPAR γ this was Leu and for PPAR δ the longer Met (Figure 16A). We imagined that the binding pocket of the PPAR γ LBD hosting the side chain alkyl group of our propanoic acid moiety was narrower and deeper. To match the situation, we designed and synthesized compounds with a benzyl group and the related substituent as the side chain alkyl group of the α -position of the phenylpropanoic acid moiety (Figure 16B). We found that a benzyl group was preferable for a PPAR γ -selective agonist.

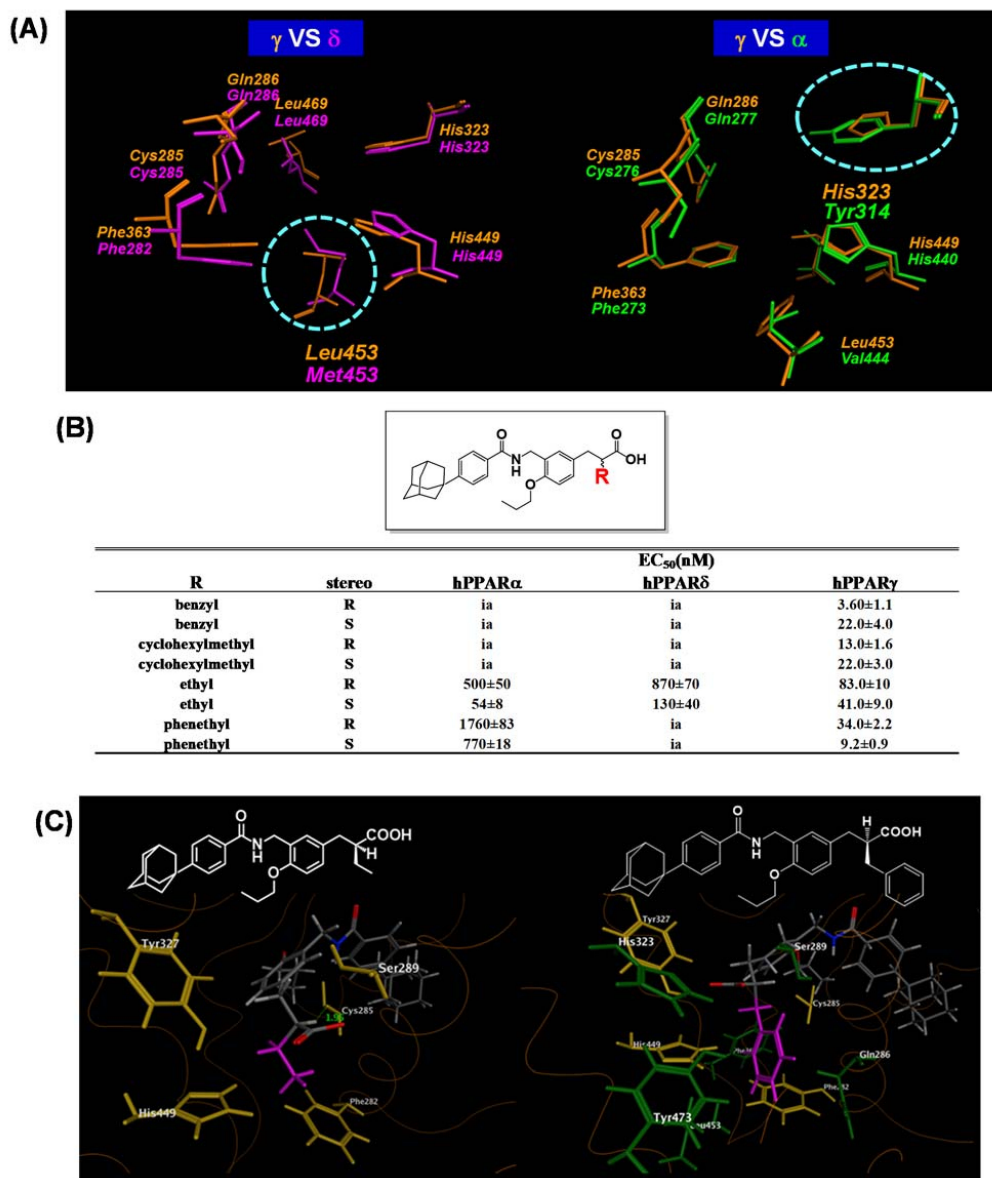
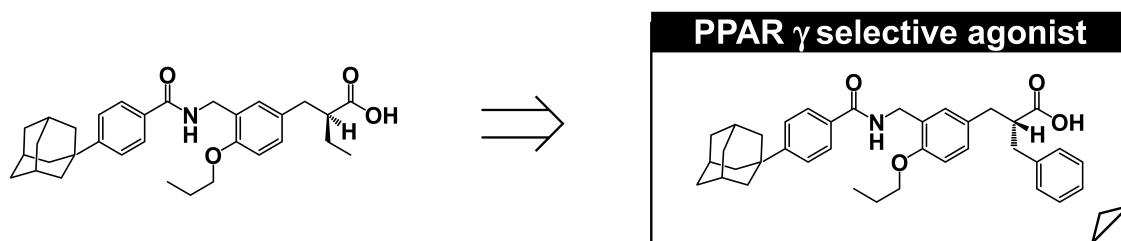


Figure 16. (A) Zoomed views of the superposed amino acid residues composing the benzyl group-binding pockets. (left) Superposition of the PPAR δ LBD (magenta) and PPAR γ LBD (orange). (right) Superposition of the PPAR γ LBD (orange) and PPAR α LBD (green). Protein backbones are omitted, and the side-chain amino acids are represented as cylinder models. (B) PPAR transactivation activity for a series of compounds. (C) Zoomed views of the amino acids involved in the interaction of the side chain of the ligands. (left) Zoomed view of the PPAR γ LBD-TIPP-703 complex. (right) Zoomed view of the PPAR γ LBD-MO-3S complex. Proteins are represented as wireframe models and the amino acids interacting with the side chain ethyl group of TIPP-703 are depicted as yellow cylinders, and the additional interacting amino acid side chains are depicted as green cylinders.



We identified a proper substituent at the α -position for PPAR γ -selective activity. However, to our surprise, the stereo-selectivity of the α -benzyl phenyl propanoic acid agonist activity for PPAR γ was different. The (*R*)-enantiomer (MO-4R) was a more potent PPAR γ -selective agonist than the antipodal (*S*)-enantiomer (MO-3S). The EC₅₀ values of MO-4R and MO-3S transactivation activities for PPAR γ were 3.60 and 22.0 nM, respectively. Consistently, MO-4R was more potent at inducing 3T3-L1 adipocyte differentiation than MO-3S (Figure 17A).

The structure–activity relationship from our PPAR agonist study indicated that the (*S*)-enantiomer was more potent than the (*R*)-enantiomer. To understand the preference of the benzyl group and the reversal of stereo-selectivity, we performed X-ray crystallographic analysis of both MO-4R and MO-3S complexed with the human PPAR γ LBD, and compared the results with those obtained from TIPP-703. As mentioned above, the α -ethylphenylpropanoic acid derivative, TIPP-703, transactivated all PPAR subtypes, while the α -benzylphenylpropanoic acid derivatives, MO-3S and MO-4R, specifically transactivated PPAR γ more potently than TIPP-703. These differences in selectivity and activity can be attributed to differences in the interaction potential of the phenylpropanoic acid side chain α -position with the surrounding amino acids. As expected, the volume of the α -substituent-binding pocket of human PPAR δ was smaller than that of human PPAR α because of the bulky Met residue (Val in human PPAR α) located at the bottom of the pocket. The bulky benzyl side chain of MO-3S might not fit into the pocket of human PPAR δ because of steric interference with the Met residue. Additionally, the width of the entrance of the human PPAR α pocket is smaller than that of human PPAR δ because of the bulky Tyr residue (His in human PPAR δ) located at the entrance of the pocket. The bulky benzyl side chain of MO-3S might not be able to enter the pocket of human PPAR α due to steric hindrance. These results explain why PPAR γ agonist activity is improved by exchanging the side chain at the α -position of phenylpropanoic acids. For TIPP-703, the ethyl group interacts with the hydrophobic cavity composed of Phe282, Cys285, Ser289, Tyr327 and His449. However, for MO-3S, the benzyl group is wider than the ethyl group and, therefore, the benzyl group interacts further with the additional hydrophobic cavity composed of Gln286, His323, Phe363, Leu453 and Tyr473. This expansion of the interaction space might be the primary reason for the increase in MO-3S activity compared with that of TIPP-703 (Figure 16C).

Contrary to our expectations, the three-dimensional structures of bound MO-3S and MO-4R closely resemble each other (Figure 17B). The only difference is in the direction of the methylene chain and the configuration of the benzene ring of the α -substituent benzyl group. Surprisingly, although the stereochemistry is opposite between MO-3S and MO-4R, the benzyl side chain of both ligands is located in the same hydrophobic pocket of the human PPAR γ LBD formed by H3, H5, H7, H11 and H12 (Figure 17B). We focused on Ser289 and Leu469 in the human PPAR γ LBD complexed with MO-3S or MO-4R because Ser289 is the closest amino acid to the methylene chain and Leu469 is the closest amino acid to the distal benzene ring of the side-chain benzyl group of both MO-3S and MO-4R. A short contact between the 2-position hydrogen atom of the MO-3S benzyl group and the oxygen atom of the Ser289 side chain was observed, together with a short contact between the 3-position hydrogen atom of the MO-3S benzyl group and the hydrogen atom of the Leu469 side chain. However, such short contacts were not observed for MO-4R. This may be one reason why MO-3S is a weaker human PPAR γ agonist than MO-4R (Figure 17C).

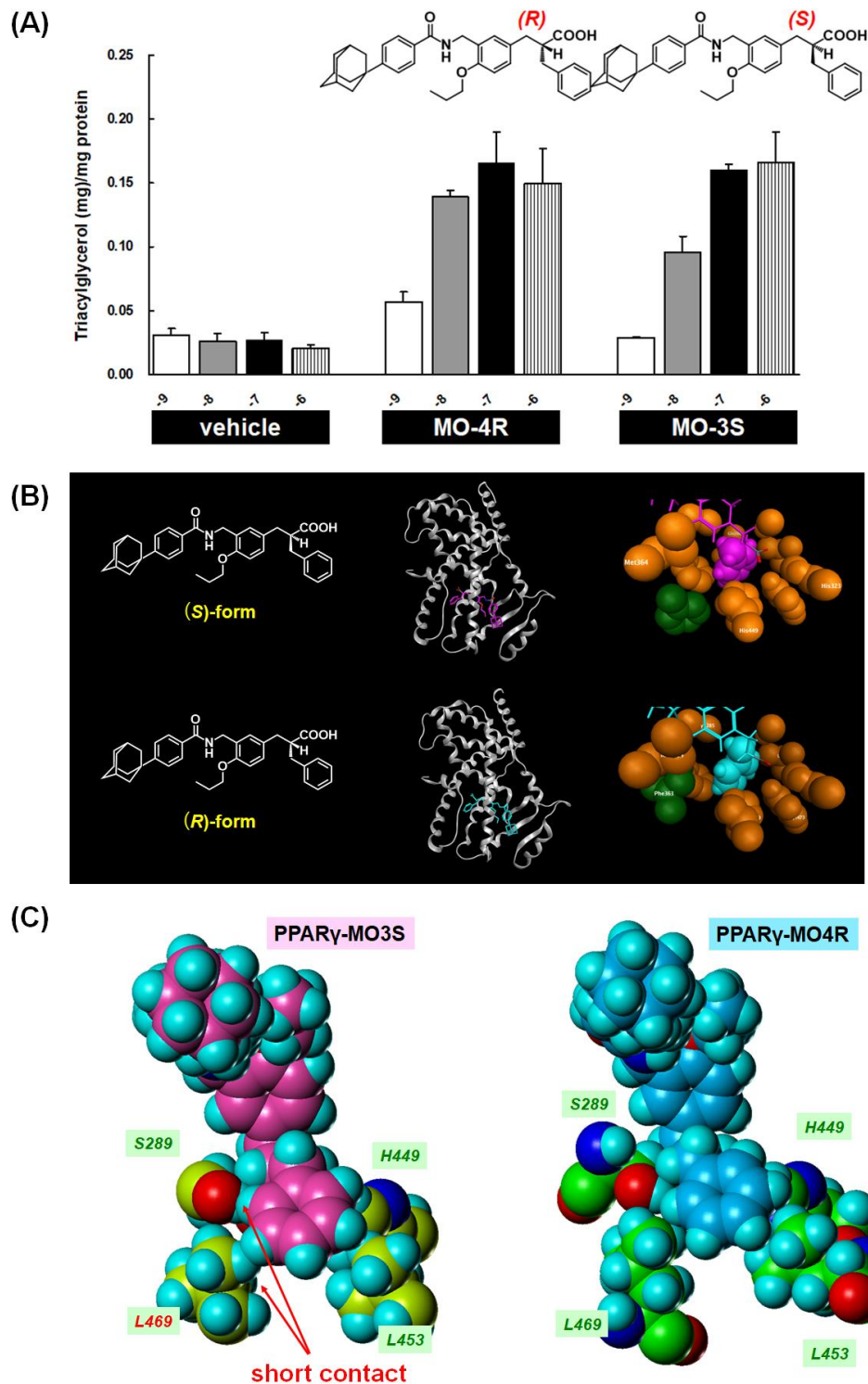
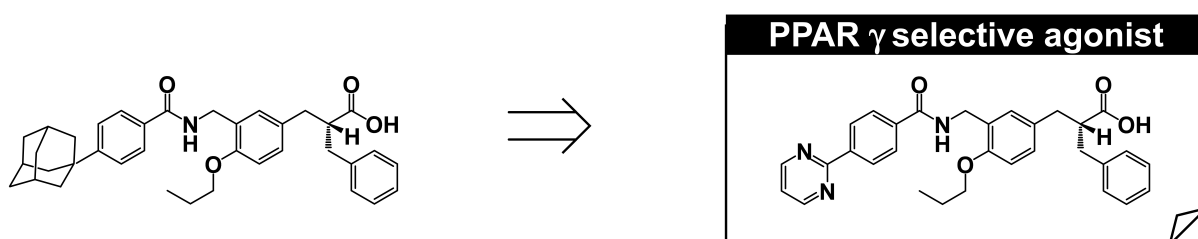


Figure 17. (A) Dose-dependent induction of 3T3-L1 adipocyte differentiation by MO-4R and MO-3S. Data are expressed as the mean with SD ($n = 3$). (B) Overall crystal structures of hPPAR γ LBD-MO-3S (MO-4R) complexes, and zoomed views of the amino acids of the hPPAR γ LBD involved in the interaction with the side-chain benzyl group of the ligands. The amino acids and the side-chain benzyl groups are depicted as space filling models in orange (interacting amino acids), magenta (benzyl group of MO-3S), and cyan (benzyl group of MO-4R). The flipped Phe363s are highlighted in green. (C) Zoomed views of the benzyl-binding pocket of hPPAR γ LBD-MO-3S and hPPAR γ LBD-MO-4R complexes. The four interacting amino acids are indicated.

12. PPAR γ -Partial Agonist: MEKT-21

We have created MO-4R, a structurally new and very potent PPAR γ -selective agonist, that is distinct from the well-known TZD class PPAR γ -selective agonists. We therefore started an anti-cancer drug-development project for MO-4R. We performed various evaluations; however, to our disappointment, we were unable to prepare sufficiently high concentrations of MO-4R in aqueous solution for toxicological studies. We temporarily suspended our project and turned our attention to improvement of the aqueous solubility of MO-4R. Aqueous solubility of compounds is an important issue in medicinal chemistry research, especially during structural development and/or structural optimization because this parameter must be optimized to ensure the drug possesses suitable *in vivo* pharmacological activity.



To create soluble phenylpropanoic acid-type PPAR γ -selective agonists, we re-focused on the substituent at the hydrophobic tail. The poor aqueous solubility of MO-4R might be primarily attributed to the presence of an adamantyl group in the hydrophobic tail, even though this substituent is the critical determinant for potent human PPAR γ -selective agonism. We have successfully created biphenylcarboxylic acid-type human PPAR δ agonists with improved aqueous solubility [59]. This improved solubility was attributed to two factors, disruption of molecular planarity and decreased hydrophobicity via introduction of a heteroaromatic ring. We applied the same strategies to the present work and found that a pyrimidine-2-yl group (MEKT-21) was preferable (Figure 18A). MEKT-21 exhibited an approximately 10,000-fold increased aqueous solubility, as judged from the calculated log(partition coefficient). In accordance with this, MEKT-21 was eluted more quickly than MO-4R. MO-4R exhibited extremely poor aqueous solubility (<1 $\mu\text{g}/\text{mL}$), but MEKT-21 improved the solubility to 301 $\mu\text{g}/\text{mL}$. We selected MEKT-21 for further evaluation, based on its activity towards human PPAR γ and good aqueous solubility.

It is interesting to note that evaluation of intrinsic MEKT-21 activity indicated that it is a partial agonist, not a full agonist; PPAR γ was activated to approximately 65% of the maximum activity achieved with the full-agonist, pioglitazone (Figure 18B).

To investigate the potential of the PPAR γ partial agonist MEKT-21 as an anti-scirrhous gastric cancer agent, we compared the apoptosis-inducing effects of MEKT-21 and MO-4R, together with the human PPAR γ full agonist, troglitazone, on the human scirrhous gastric cancer cell line OCUM-2MD3 [60]. Troglitazone was used as a positive control because it suppresses the growth of gastric cancer cell lines, such as MKV45 [61], SNU-216 and SNU-668 cells [62]. Troglitazone dose-dependently enhanced apoptosis in the concentration range 1–100 μM . Therefore, troglitazone induced apoptosis of OCUM-2MD3 cells but had little effect on normal cells. The human PPAR γ full agonist, MO-4R, also dose-dependently enhanced apoptosis in the concentration range 1–100 μM , and it was more potent than troglitazone (10 μM MO-4R effectively induced apoptosis of OCUM-2MD3 cells). However, 100 μM MO-4R induced apoptosis of both OCUM-2MD3 and OCUM-24 cell lines. Therefore, MO-4R has poorer selectivity for human scirrhous gastric cancer cells compared with troglitazone (Figure 18C).

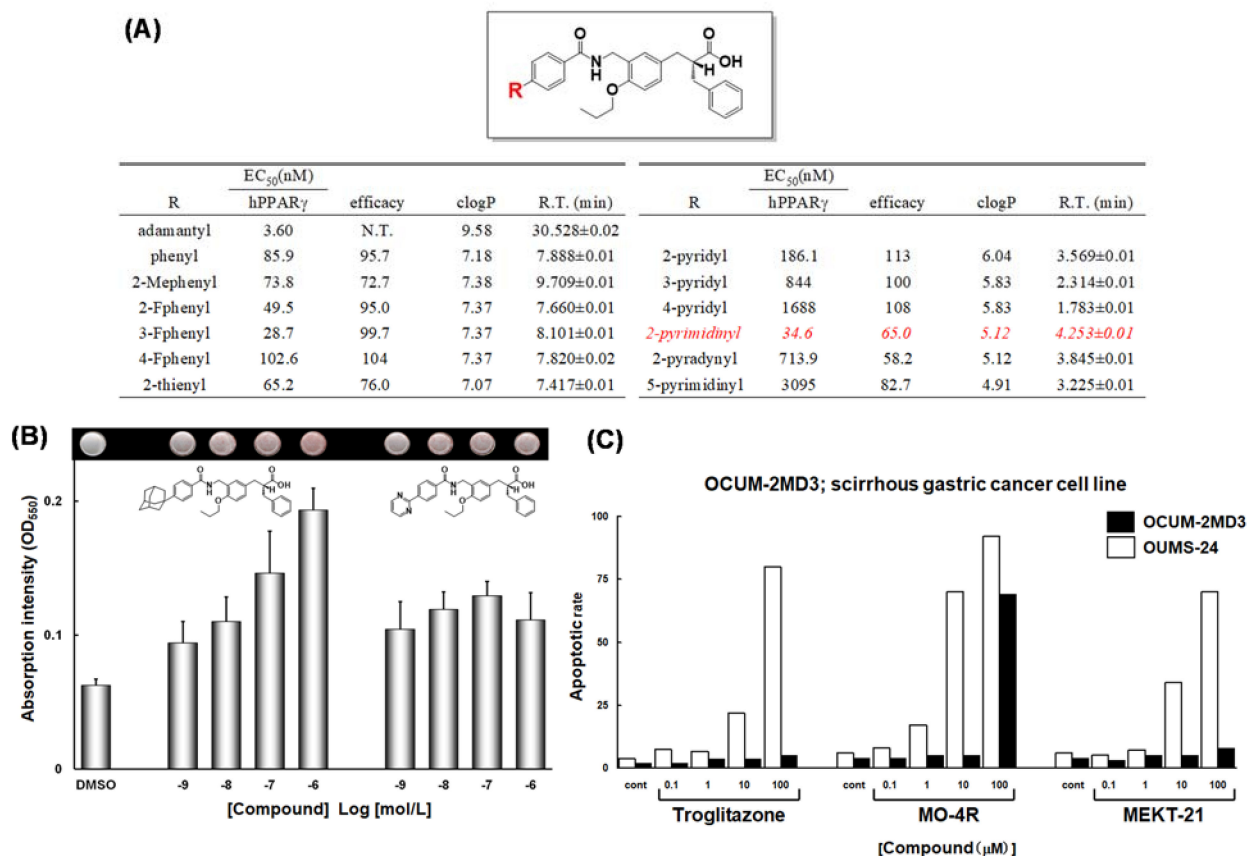


Figure 18. (A) PPAR_γ agonist activities of a series of compounds. (B) Adipogenesis-inducing activity of MO-4R and MEKT-21. After pretreatment with 1 l M Dex, 0.5 mM IBMX, and 5 μg/mL insulin, 3T3-L1 cells were incubated with the indicated concentrations of MO-4R and MEKT-21. Oil red O-stained cells are shown at the top and are quantified at the bottom by measurement of OD550 (±SD). (C) Apoptosis-inducing activity of troglitazone, MO-4R and MEKT-21 in OCUM-2MD3 and OUMS-24 cells.

The human PPAR_γ partial agonist, MEKT-21, also dose-dependently induced apoptosis of OCUM-2MD3 cells in the concentration range 1–100 μM. Its potency was equal to or somewhat greater than that of troglitazone (based on activity at 10 μM). Furthermore, MEKT-21 showed high selectivity for cancer cells, comparable to that of MO-4R. These results indicated that partial activation of PPAR_γ might be sufficient to induce apoptosis of human scirrhous gastric cancer cells.

X-ray crystallography (Figure 19) clearly revealed the reason for this difference. The pyrimidin-2-yl ring and adamantyl ring are hosted in the same binding pocket, i.e., the large Y3 arm cavity composed of the side chains of amino acid residues Leu255, Glu259, Ile262, Phe264, Arg280 and Ile281. The planar pyrimidin-2-yl ring can interact less effectively with this large hydrophobic cavity compared with the three-dimensionally expanded hydrophobic adamantyl ring, especially with regard to hydrophobic interactions with Ile262, Phe264, and Ile 281, which are positioned on both sides of the pyrimidin-2-yl ring of MEKT-21 (Figure 19D–G).

The qualitative characteristics of corepressor dissociation and coactivator recruitment of nuclear receptors are regulated differentially by the three-dimensional structure around the C-terminal H12 and the surrounding helices [63]. In the binding of a full agonist, such as rosiglitazone, H12 forms part of the coactivator-binding surface, along with H3 and H5 [64]. In this case, the positions and directions of the side chains of two distinct hydrophilic amino acids, Lys301 (in H3) and Glu471 (in H12), are critically important because these amino acids clamp the LXXLL motif (L, leucine; X, any amino acid) of the coactivator, and dock it appropriately to express full-agonistic activity. Therefore, we

compared the three-dimensional structures of two PPAR γ full agonists, rosiglitazone and farglitazar [65], complexed with the PPAR γ LBD (Figure 20A–D). The overall folds are well matched and the positions and the directions of the side chains of Lys301 and Glu471 overlap well in these structures. The root mean square deviations (RMSDs) of these two amino acid residues are 0.71 Å and 0.44 Å, respectively (Figure 20E,F). These results indicate that the two PPAR γ full agonists can recruit coactivator complexes with almost the same efficacy, eliciting full agonistic activity.

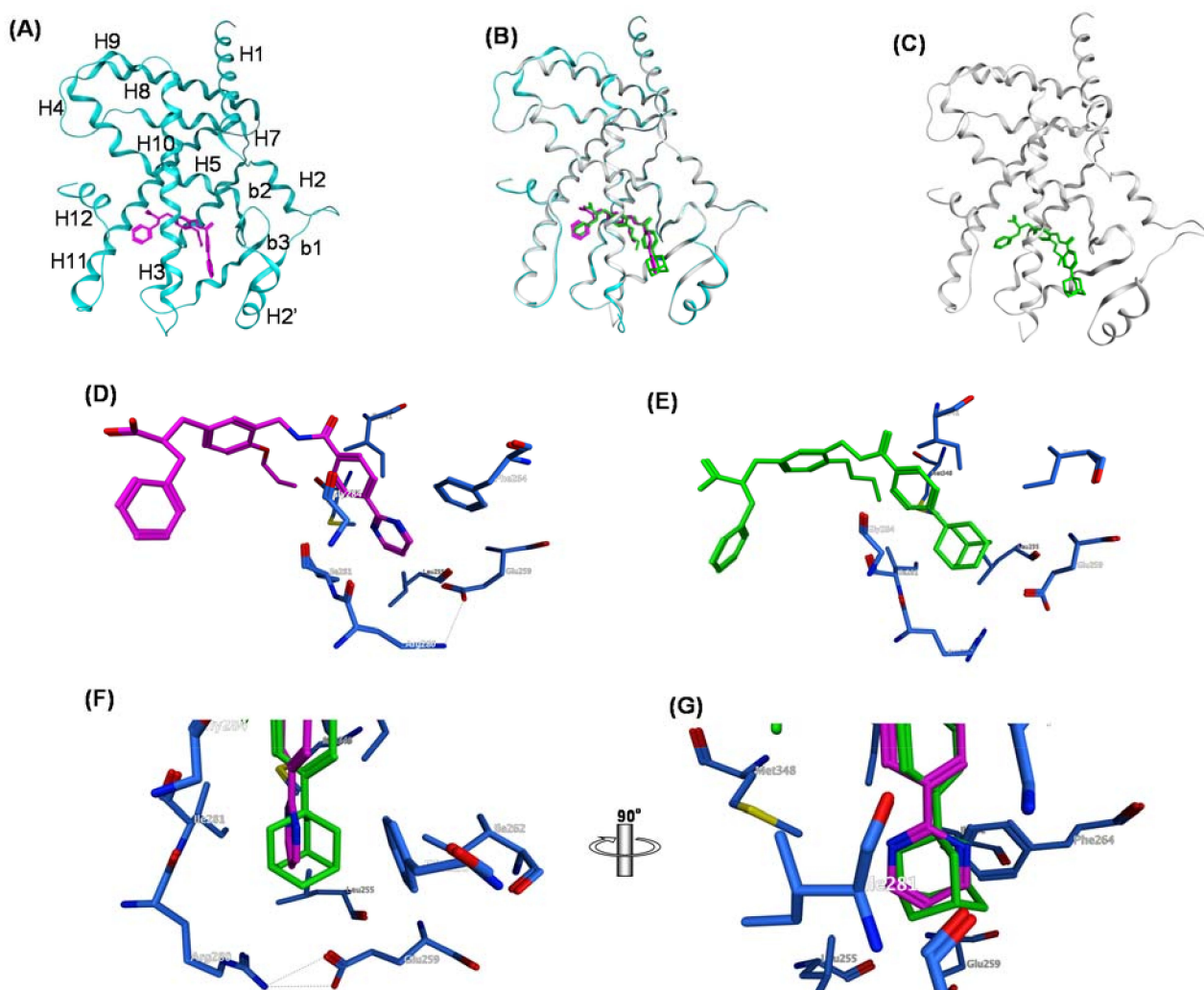


Figure 19. (A–G) Crystal structures of hPPARcLBD–MO-4R and hPPARcLBD–MEKT-21 complexes. (A) Structure of the whole hPPARcLBD–MEKT-21 complex. Protein is represented by a blue ribbon model and MEKT-21 is depicted with a magenta cylinder model. The numbering of the second structure is also depicted. The nomenclature of the helices is based on the RXR- α crystal structure. (B) The superimposed structures of MO-4R and MEKT-21 complexed with the hPPARcLBD. (C) Structure of the whole hPPAR χ LBD–MO-4R complex. Protein is represented by a white ribbon model and MO-4R is depicted with a green cylinder model. (D) Zoomed view of the binding mode of the hydrophobic tail part of MO-4R in the Y3 arm. The side chains of amino acids of the Y3 arm are depicted by blue cylinder models. (E) Zoomed view of the binding mode of the hydrophobic tail of MEKT-21 in the Y3 arm. (F) Zoomed view of the alignment of the hydrophobic tail of MO-4R and MEKT-21. (G) Image F rotated by 90 degrees.

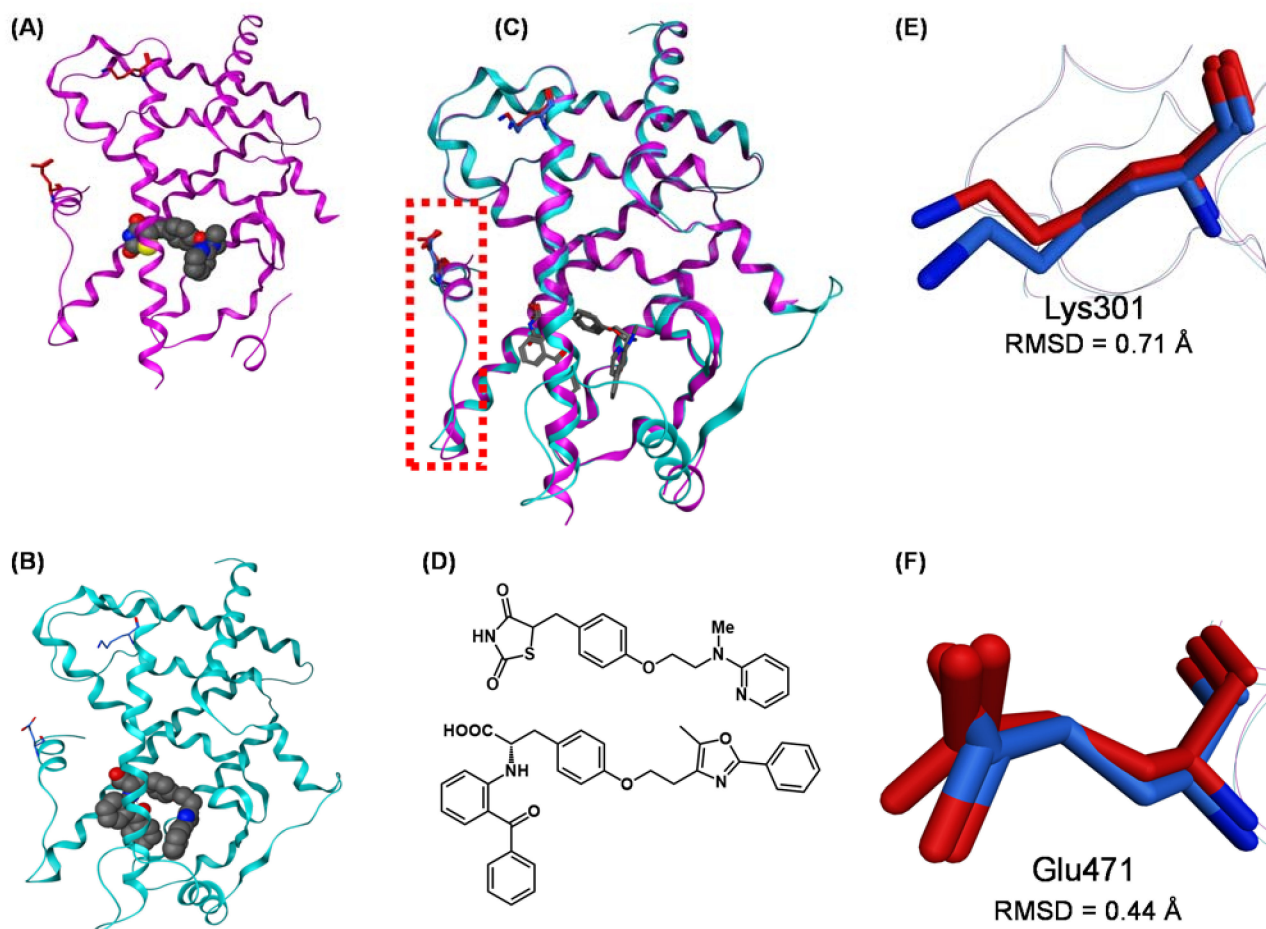


Figure 20. (A,B) Crystal structures of hPPAR γ LBD–rosiglitazone (full agonist) complex (PDB: 2PRG) and hPPAR γ LBD–farglitazar (full agonist) complex (PDB: 1FM9). (C) The superimposed structures of hPPAR γ LBD–rosiglitazone and hPPAR γ LBD–farglitazar complexes. Both ligands are depicted as cylinder models, and Lys301 and Glu473 are highlighted as cylinder models in magenta (rosiglitazone complex) and cyan (farglitazar complex). The N-terminal AF2 region (H12 helix) is highlighted by a light red dotted box. (D) Chemical structures of rosiglitazone and farglitazar. (E) Zoomed view of the superimposed Lys301 of the hPPAR γ LBD–rosiglitazone complex and hPPAR γ LBD–farglitazar complex. Lys301 is highlighted as a cylinder model in magenta (rosiglitazone complex) or blue (farglitazar). (F) Zoomed view of the superimposed Glu473 of the hPPAR γ LBD–rosiglitazone complex and hPPAR γ LBD–farglitazar complex. Glu473 is highlighted as a cylinder model in magenta (rosiglitazone complex) or blue (farglitazar). Lys301 residues are highlighted as a green cylinder model.

However, the overall structures of the PPAR γ LBD complexed with PPAR γ partial agonists, including MEKT-21, are somewhat different. The frameworks of the PPAR γ LBD complexed with several representative PPAR γ partial agonists (MEKT-21, LT127 [66], phenoxyacetic acid compound [67], GW-0072 [68], pyrazole compound [69], and GQ-16 [70]) are depicted in Figure 21A–F, and in a superposition in Figure 21G. The folds of the upper half of the PPAR γ LBD are well matched in these complexes. However, the folds of the lower half of the PPAR γ LBD are somewhat different. The position of Lys301 in H3 varies somewhat in these structures (RMSD = 1.10 Å compared with 0.71 Å for full agonists). However, the side chain of Glu471 in H12 faces in various directions in these complexes, and the RMSD is much larger (1.89 Å compared with 0.44 Å for full agonists). These substantial differences in structure might be one of the driving forces behind the partial agonistic activity of these compounds, including MEKT-21.

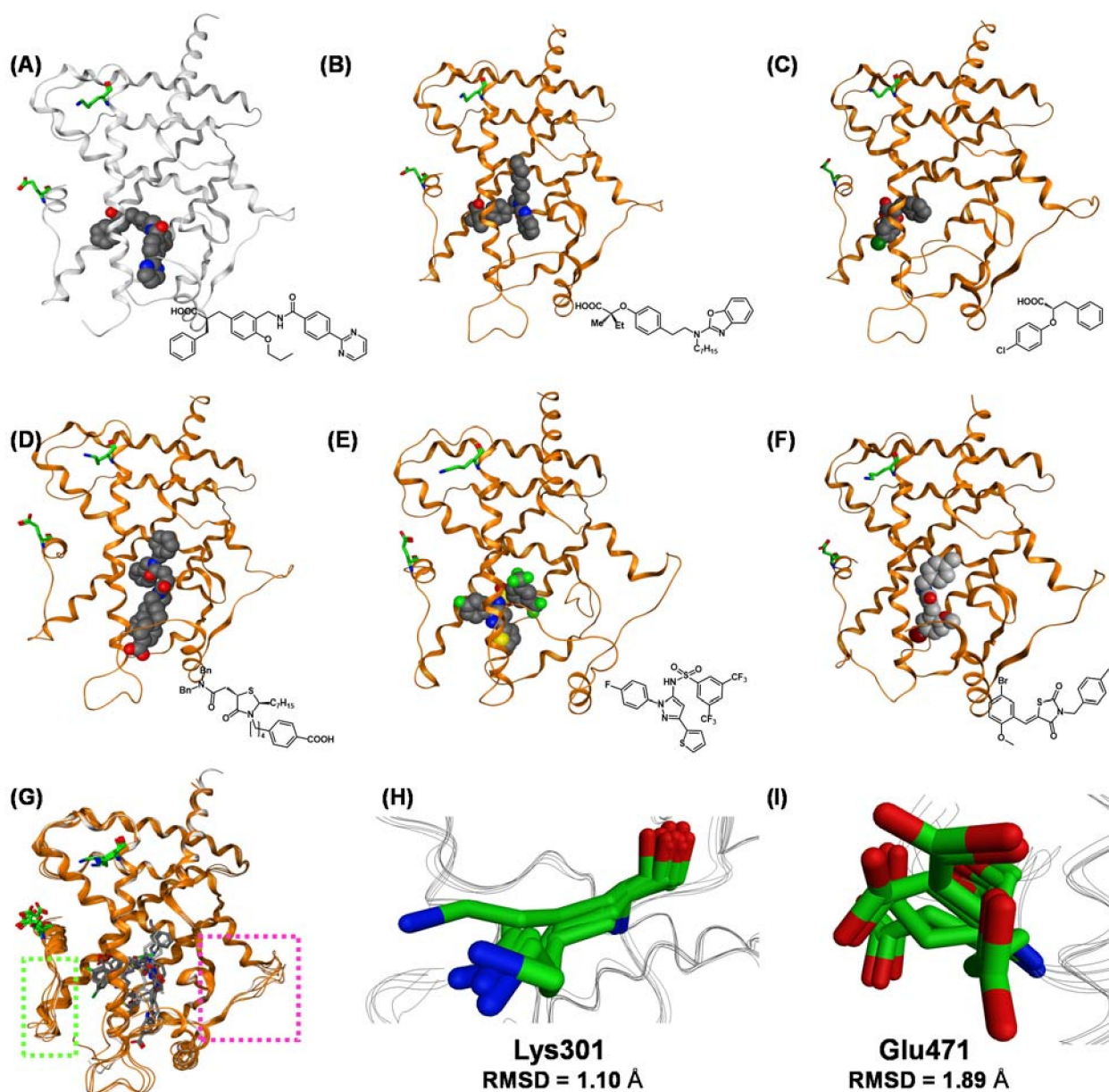


Figure 21. (A–F) Crystal structures of hPPAR γ LBD–partial agonist complexes. (A) Crystal structure of the hPPAR γ LBD–MEKT-21 complex (PDB: 3VSO). (B) Crystal structure of the hPPAR γ LBD–LT127 complex (PDB: 2I4Z). (C) Crystal structure of the hPPAR γ LBD–(2S)-2-(4-chlorophenoxy)-3-phenylpropanoic acid complex (PDB: 3CDP). (D) Crystal structure of the hPPAR γ LBD–GW-0072 complex (PDB: 4PRG). (E) Crystal structure of the hPPAR γ LBD–N-[1-(4-fluorophenyl)-3-(2-thenyl)-1H-pyrazole-5-yl]-3,5-bis(trifluoromethyl)benzenesulfonamide complex (PDB: 2GOH). (F) Crystal structure of the hPPAR γ LBD–GQ-16 complex (PDB: 3T03). (G) The superimposed structures of hPPAR γ LBD–partial agonist complexes. All ligands are depicted as cylinder models, and Lys301 and Glu471 are highlighted as green cylinder models. The N-terminal AF2 region (H12 helix) is highlighted with a light green dotted box. (H) Zoomed view of the superimposed Lys301 of hPPAR γ LBD–partial agonist complexes. (I) Zoomed view of the superimposed Glu471 of hPPAR γ LBD–partial agonist complexes.

To further understand the key differences in the binding of full and partial PPAR γ agonists, we focused on the binding mode of these agonists to Tyr473 in H12. Tyr473 is believed to play a critical role in the full agonist-mediated stabilization of the LBD of PPAR γ (Figure 22A–C). For rosiglitazone, the side chain phenol oxygen of Tyr473 forms a tight hydrogen bond with the nitrogen atom of the thiazolidine-2,4-dione ring. Furthermore, the side chain phenol oxygen of Tyr473 has a hydrogen bond interaction with the carbonyl oxygen atom of the thiazolidine-2,4-dione ring. These hydrogen bond

networks tightly fix Tyr473 in H12, forming a section of the transcriptional coactivator-binding surface (Figure 22A).

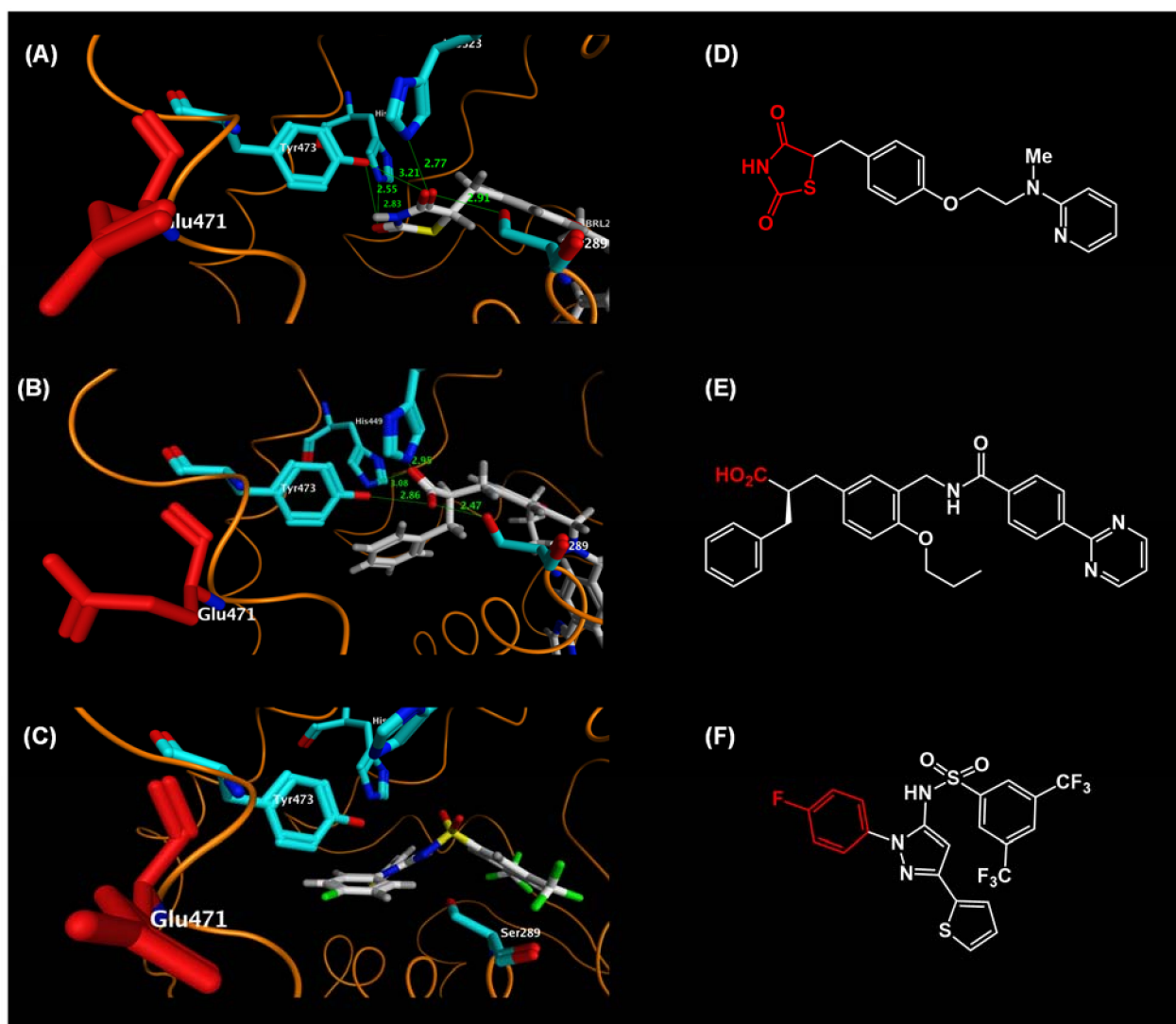


Figure 22. (A–C) Zoomed views of the binding mode of the AF2 region (H12 helix) of hPPAR γ LBD–rosiglitazone. (A) Zoomed view of the hPPAR γ LBD–rosiglitazone (full agonist) complex. (B) Zoomed view of the hPPAR γ LBD–MEKT-21 (partial agonist) complex. (C) Zoomed view of the hPPAR γ LBD–*N*-[1-(4-fluorophenyl)-3-(2-thenyl)-1*H*-pyrazole-5-yl]-3,5-bis(trifluoromethyl)benzenesulfonamide (partial agonist) complex. (D–F) Chemical structures of these agonists. (D) rosiglitazone, (E) MEKT-21, and (F) *N*-[1-(4-fluorophenyl)-3-(2-thenyl)-1*H*-pyrazole-5-yl]-3,5-bis(trifluoromethyl)benzenesulfonamide.

In the partial agonist, *N*-[1-(4-fluorophenyl)-3-(2-thenyl)-1*H*-pyrazole-5-yl]-3,5-bis(trifluoromethyl)benzenesulfonamide [Protein Data Bank (PDB): 2GOH], the 4-fluorophenyl group is located close to H12, but it has no hydrophobic or hydrogen bond interaction with this helix and there is no significant ligand-mediated interaction to fix Tyr473 in H12. The absence of interaction with Tyr473 in H12 might provide the structural basis for the partial agonist functionality of not only this compound, but also the other neutral-and carboxylic acid-type PPAR γ partial agonists (Figure 22C).

The acidic carboxylic acid moiety of α -benzylphenylpropanoic acid MEKT-21 hydrogen bonds with the side chain phenol oxygen of Tyr473. However, the distance between these two functionalities is longer than that of the PPAR γ LBD complexed with the thiazolidine-2,4-dione-type PPAR γ full agonist, rosiglitazone. Furthermore, there is only a single hydrogen bond between the acidic moiety of MEKT-21 and Tyr473 in H12. Tyr473

in H12 is thought to be fixed less effectively when MEKT-21 is bound to the PPAR γ -LBD, resulting in partial agonistic activity (Figure 22B).

13. Structural Basis of Full and Partial PPAR γ Agonists

TZD class full PPAR γ agonists are widely used for the treatment of type 2 diabetes. However, TZDs possess adverse side effects, including significant weight gain, peripheral edema, bone loss and increased risk of congestive heart failure, which are associated with over-activation of PPAR γ [71]. Recently, attention has turned to partial PPAR γ agonists, which activate PPAR γ less than maximally.

We created the partial PPAR γ agonist, MEKT-21. The exact mechanism by which MEKT-21 exhibits partial PPAR γ agonism is not fully understood; however, based on clinical need, we aimed to design and synthesize further partial PPAR γ agonists. Based on the NR transactivation mechanism, an H12 holding inducer is a full NR agonist. We noted that a tight hydrogen bond network is critical to induce proper H12 holding for maximum activity of PPAR γ agonists. Therefore, we predicted that replacement of the PPAR γ agonist carboxyl group with another weak acidic functionality, such as acylsulfonamide, might result in partial PPAR γ agonists [72]. An acylsulfonamide group interacted with Tyr473 moderately to partially stabilize H12 of the PPAR γ LBD. We modified the structure of the full agonist, TIPP-703, to remove the carboxyl group and to introduce an acylsulfonamide group to obtain MEKT-75 (Figure 23A).

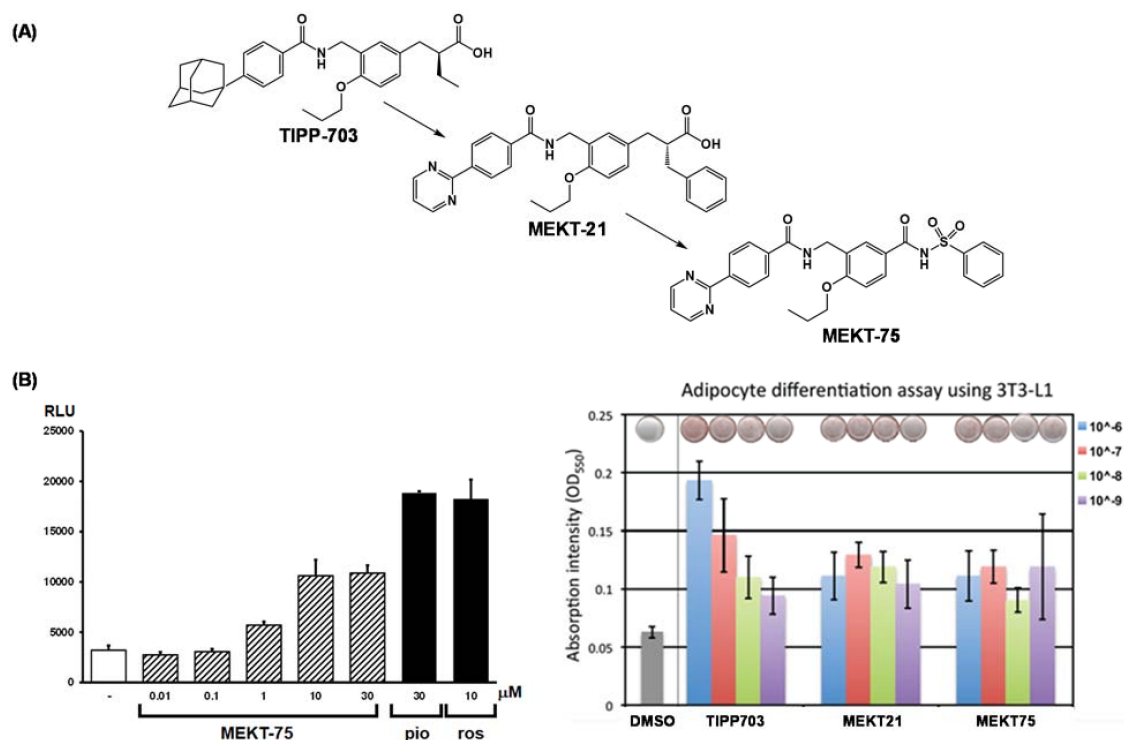


Figure 23. (A) Structural development of a hPPAR γ -selective partial agonist from a hPPAR γ pan agonist. (B) (left) Transactivation activity of MEKT-75, pioglitazone (pio) and rosiglitazone (ros). (right) Adipocyte differentiation assay of TIPP-703, MEKT-21 and MEKT-75. Homo-dimeric structure of MEKT-75 complexed with the hPPAR γ LBD.

As expected, MEKT-75 exhibited apparent transactivation activity, although without clear dose-dependency, and its maximal activity was approximately 50% of the maximal response of the positive controls (Figure 23B). These results are consistent with the idea that MEKT-75 is a partial PPAR γ agonist.

We solved the X-ray crystallographic structure of MEKT-75 complexed with the PPAR γ LBD homodimer (Figure 24A–L). The crystal was obtained by soaking a crystal of the homodimer in ligand solution. Each PPAR γ LBD in the homodimer binds one molecule

of MEKT-75. Interestingly, the structural folding of the LBD remains almost unchanged, except for the region from the end of H11 to the C-terminal H12 region. Furthermore, the structural folds in one part of the homodimer structure are almost identical to those in the PPAR γ LBD–rosiglitazone complex (Figure 24B), whereas those in the other part of the homodimer structure are different (Figure 24C). Therefore, we tentatively designated the former structure as the fully active form of the PPAR γ LBD, and the latter structure as a non-fully active form.

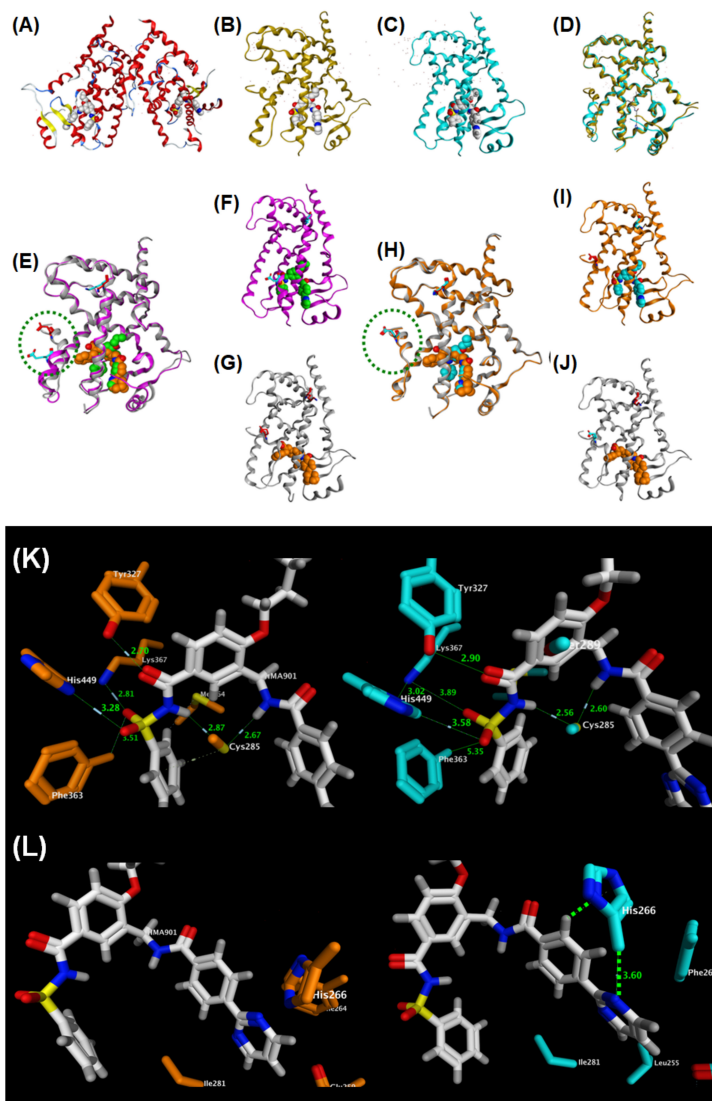


Figure 24. (A) Structural development of a hPPAR γ -selective partial agonist from a hPPAR γ pan agonist. (B–E) X-ray crystallographic structure of the homo-dimeric structure of MEKT-75 complexed with the hPPAR γ LBD. (B) Homo-dimeric structure of MEKT-75 complexed with the hPPAR γ LBD. (C) Full agonist form monomer. (D) Partial agonist form monomer. (E) Superposed structure of the homo-dimeric structure of MEKT-75 complexed with the hPPAR γ LBD. MEKT-75 was omitted. (F) Superposed structure of the partial agonist form MEKT-75 monomer and the TIPP-703 monomer complexed with the hPPAR γ LBD. (G) Partial agonist form MEKT-75 monomer. (H) Overall structure of TIPP-703 complexed with the hPPAR γ LBD. (I) Superposed structure of the full agonist form MEKT-75 monomer and the TIPP-703 monomer complexed with the hPPAR γ LBD. (J) Partial agonist form MEKT-75 monomer. (K,L) (left) Zoomed view of the fully active form of MEKT-75. (right) Zoomed view of the non-fully active form of MEKT-75.

In the fully active form, MEKT-75 takes a U-shaped structure, similar to that of TIPP-703. The acylsulfonamide group of MEKT-75 is positioned near H11. A hydrogen bond network involving five amino acids, Ser289, His323, Tyr327, His449 and Tyr473, is formed in the interaction of full agonists with the LDB. Therefore, interactions of three of these five amino acids are conserved in the one LDB complexed with MEKT-75. This appears to be sufficient to support the fully active LDB structure [Figure 24K,L (left)]. In contrast, in the non-fully active LDB, another interaction was noted: His266 is located close to the (pyrimidin-2-yl)phenyl moiety of MEKT-75, resulting in hydrophobic interaction between His266 and the phenyl group, and between the His266 and the pyrimidin-2-yl group. These additional interactions cause the bound MEKT-75 to move to the right, so that the distance from the phenylsulfonamylcarbonyl group of MEKT-75 to the side chains of Ser289, Tyr327, Lys367, His449 and Phe363 becomes longer. As a result, the hydrogen bond network is weaker, which may mean that the H12 region is not restricted to the appropriate location for full activity [Figure 24K,L (right)].

We checked the X-ray crystallographic structure of the PPAR γ LBD apo-form (without ligand). The PPAR γ LBD apo-form also forms a homodimer in which one LBD is in the fully active form, and the other is in a non-fully active form [Figure 26A (center)]. This indicates that two types of PPAR γ LBD structures are present in the crystal state, irrespective of the presence or absence of agonist. Indeed, the apo-form PPAR γ LBD homodimer and the ligand-bound PPAR γ LBD homodimer did not show apparent structural differences in the LBD, indicating that partial agonists lack the ability to induce a fully active LBD [Figure 26A (left)].

In contrast, the PPAR γ LBD-rosiglitazone complex also formed a homodimer in the crystal, but each LBD was present in a fully active form [Figures 25A and 26A (right)]. This result indicates that full agonists do induce structural change of the non-fully active PPAR γ LBD to a fully active LBD, presumably by facilitating a tight hydrogen bond network with the LBD. We speculate that there is a dynamic equilibrium between the fully active and non-fully form of the PPAR γ LBD.

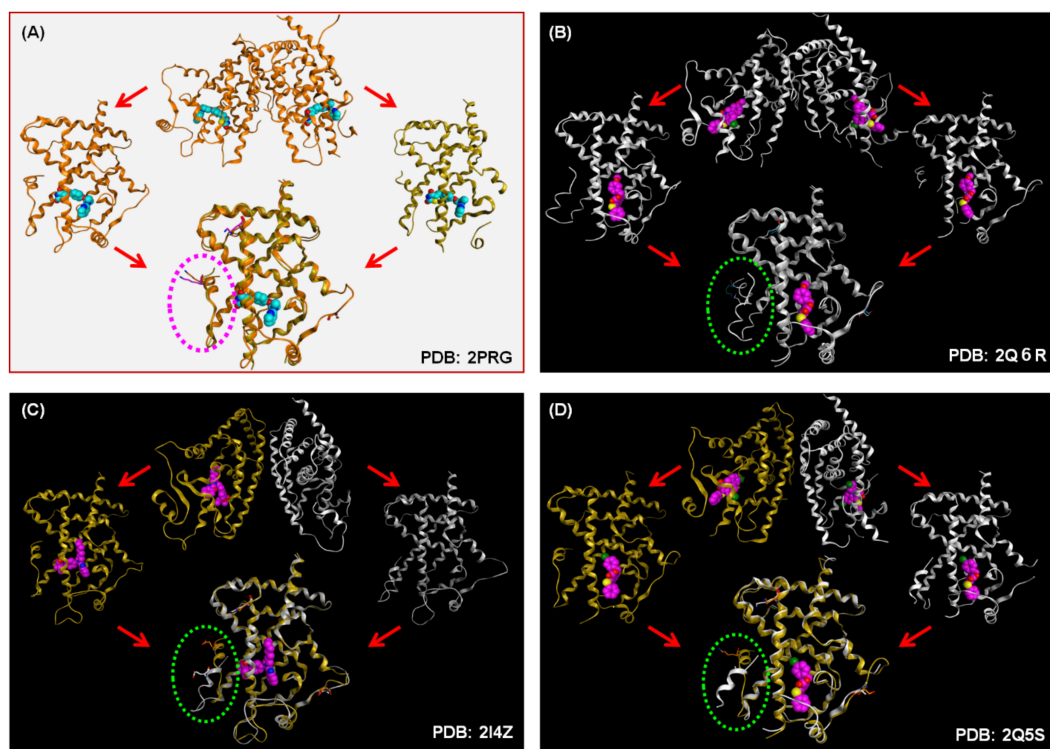


Figure 25. (A) X-ray crystallographic structure of homo-dimeric PDB: 2PRG (full agonist). (B) X-ray crystallographic structure of homo-dimeric PDB: 2Q6R (partial agonist). (C) X-ray crystallographic structure of homo-dimeric PDB: 2I4Z (partial agonist). (D) X-ray crystallographic structure of homo-dimeric PDB: 2Q5S (partial agonist).

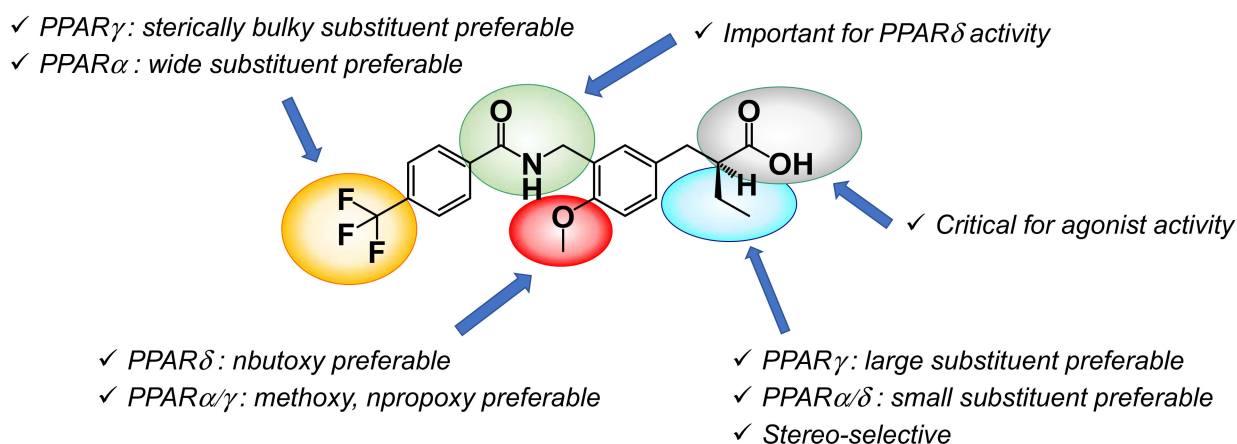


Figure 27. Structure–activity relationship summary of the present series of compounds.

We think the present strategy is applicable to the development of other nuclear receptor agonists/partial agonists because the structural similarity of LBDs in the various nuclear receptors is high. In support of this, we have succeeded in creating vitamin D receptor agonists [75,76], and farnesoid X receptor agonists [77,78].

Furthermore, considering the ligand-mediated activation mechanism of action, the present strategy is also applicable to NR antagonist design. Accordingly, we have also been engaged in the design and synthesis of NR antagonists for PPAR δ [79], PPAR γ [80], LXR [81,82], farnesoid X receptor [78], and progesterone receptor [83]. These results will be disclosed in the near future.

Funding: This work was supported by the Targeted Proteins Research Program of the Japan Science and Technology Corporation, the Platform for Drug Discovery, Informatics, and Structural Life Science from the Ministry of Education, Culture, Sports, Science and Technology, Japan, the Uehara Memorial Foundation, the Tokyo Biochemical Research Foundation, the Okayama Foundation for Science and Technology, and a Grant in-aid for Scientific Research KAKENHI (B) (grant number 26293027 to H.M.) from the Ministry of Education, Culture, Sports, Science and Technology, Japan.

Institutional Review Board Statement: Not applicable.

Informed Consent Statement: Not applicable.

Data Availability Statement: Data sharing not applicable.

Acknowledgments: The author special thanks to Junichi Kasuga and Masao Ohashi for their synthesis and evaluation of many PPAR agonists. The author thanks all collaborators who have contributed to our published body of work. The author also thanks the SC-NMR Laboratory of Okayama University for NMR measurements.

Conflicts of Interest: The author declares no conflict of interest.

Abbreviations

ADRP	adipocyte differentiation-related protein
AF-1	transactivation function-1
AF-2	transcriptional activation function-2
ALP	alkaline phosphatase
ALT	alanine aminotransferase
ANGPTL	angiopoietin-like protein
AST	aspartate aminotransferase
CPT1A	carnitine palmitoyltransferase 1A
DR1	hexameric AGGTCA recognition motif, separated by one nucleotide
EPA	eicosapentaenoic acid
G1	gap 1

GAL4	galactosidase 4
H12	helix 12
HDL	high-density lipoprotein
HMGCS2	HMG-CoA synthase 2
LBD	ligand binding domain
NASH	nonalcoholic steato-hepatitis
NCoA	nuclear receptor corepressor
NCoR	nuclear receptor corepressor
NRs	nuclear receptors
PDB	protein data bank
PPARs	peroxisome proliferator-activated receptors
PPRE	peroxisome proliferator responsive element
RAR α	retinoic acid receptor alpha
RXR	retinoid X receptor
RMSD	root mean square deviation
SMRT	silencing mediator for retinoid or thyroid-hormone receptor
SRC-1	steroid Receptor Co-Activator-1
THF	tetrahydrofurane
TNF- α	tumor necrosis factor-alpha
TZD	thiazolidinediones
ADRP	adipocyte differentiation-related protein
AF-1	transactivation function-1
AF-2	transcriptional activation function-2
ALP	alkaline phosphatase
ALT	alanine aminotransferase
ANGPTL	angiopoietin-like protein
AST	aspartate aminotransferase
CPT1A	carnitine palmitoyltransferase 1A
DR1	hexameric AGGTCA recognition motif, separated by one nucleotide
EPA	eicosapentaenoic acid
G1	gap 1
GAL4	galactosidase 4
H12	helix 12
HDL	high-density lipoprotein
HMGCS2	HMG-CoA synthase 2
LBD	ligand binding domain
NASH	nonalcoholic steato-hepatitis
NCoA	nuclear receptor corepressor
NCoR	nuclear receptor corepressor
NRs	nuclear receptors
PDB	protein data bank
PPARs	peroxisome proliferator-activated receptors
PPRE	peroxisome proliferator responsive element

References

1. Chawta, A.; Repa, J.J.; Evans, R.M.; Mangelsdorf, D.J. Nuclear receptors and lipid physiology: Opening the x-files. *Science* **2001**, *294*, 1866–1870.
2. Banner, C.D.; Gottlicher, M.; Widmark, E.; Sjoval, J.; Rafter, J.J.; Gustafsson, J.A. A systematic analytical chemistry/cell assay approach to isolate activators of orphan nuclear receptors from biological extracts: Characterization of peroxisome proliferator-activated receptor activators in plasma. *J. Lipid Res.* **1993**, *34*, 1583–1591. [[CrossRef](#)]
3. Wagner, K.D.; Wagner, N. Peroxisome proliferator-activated receptor β/δ (PPAR β/δ) acts as regulator of metabolism linked to multiple cellular functions. *Pharmacol. Ther.* **2010**, *125*, 423–435. [[CrossRef](#)] [[PubMed](#)]
4. Keller, H.; Dreyer, C.; Medin, J.; Mahfoudi, A.; Ozato, K.; Wahli, W. Fatty acids and retinoids control lipid metabolism through activation of peroxisome proliferator-activated receptor-retinoid X receptor heterodimers. *Proc. Natl. Acad. Sci. USA* **1993**, *90*, 2160–2164. [[CrossRef](#)] [[PubMed](#)]
5. Staels, B.; Auwerx, J. Role of PPAR in the pharmacological regulation of lipoprotein metabolism by fibrates and thiazolidinediones. *Curr. Pharm. Des.* **1997**, *3*, 1–14.

6. Lim, H.; Gupta, R.A.; Ma, W.G.; Paria, B.C.; Moller, D.E.; Morrow, J.D.; DuBois, R.N.; Trzaskos, J.M.; Dey, S.K. Cyclo-oxygenase-2-derived prostacyclin mediates embryo implantation in the mouse via PPAR δ . *Genes Dev.* **1999**, *13*, 1561–1574. [[CrossRef](#)]
7. Sznajdman, M.L.; Haffner, C.D.; Maloney, P.R.; Fivush, A.; Chao, E.; Goreham, D.; Chao, E.; Goreham, D.; Sierra, M.L.; LeGrumelec, C.; et al. Novel selective small molecule agonists for peroxisome proliferator-activated receptor δ (PPAR δ) synthesis and biological activity. *Bioorg. Med. Chem. Lett.* **2003**, *13*, 1517–1521. [[CrossRef](#)]
8. Oliver, W.R., Jr.; Shenk, J.L.; Snaith, M.R.; Russell, C.S.; Plunket, K.D.; Bodkin, N.L.; Lewis, M.C.; Winegar, D.A.; Sznajdman, M.L.; Lambert, M.H.; et al. A selective peroxisome proliferator-activated receptor δ agonist promotes reverse cholesterol transport. *Proc. Natl. Acad. Sci. USA* **2001**, *98*, 5306–5311. [[CrossRef](#)]
9. Tanaka, T.; Yamamoto, J.; Iwasaki, S.; Asaba, H.; Hamura, H.; Ikeda, Y.; Watanabe, M.; Magoori, K.; Ionka, R.X.; Tachibana, K.; et al. Activation of peroxisome proliferator-activated receptor δ induces fatty acid β -oxidation in skeletal muscle and attenuates metabolic syndrome. *Proc. Natl. Acad. Sci. USA* **2003**, *100*, 15924–15929. [[CrossRef](#)]
10. Okuno, A.; Tamemoto, H.; Tobe, K.; Ueki, K.; Mori, Y.; Iwamoto, K.; Umesono, K.; Akanuma, Y.; Fujiwara, T.; Horikoshi, H.; et al. Troglitazone increases the number of small adipocytes without the change of white adipose tissue mass in obese Zucker rats. *J. Clin. Invest.* **1998**, *101*, 1354–1361. [[CrossRef](#)]
11. Huang, J.-W.; Shiau, C.-W.; Yang, J.; Wang, D.-S.; Chiu, H.-C.; Chen, C.-S.; Chen, A.C.-Y. Development of small-molecule cyclin D1-ablative agents. *J. Med. Chem.* **2006**, *49*, 4684–4689. [[CrossRef](#)]
12. Duszka, K.; Gregor, A.; Guillou, H.; König, J.; Wahli, W. Peroxisome Proliferator-Activated Receptors and Caloric Restriction—Common Pathways Affecting Metabolism, Health, and Longevity. *Cells* **2020**, *9*, 1708. [[CrossRef](#)] [[PubMed](#)]
13. Hashimoto, Y.; Miyachi, H. Nuclear receptor antagonists designed based on the helix-folding inhibition hypothesis. *Bioorg. Med. Chem.* **2005**, *13*, 5080–5093. [[CrossRef](#)]
14. Nomura, M.; Tanase, T.; Ide, T.; Tsunoda, M.; Suzuki, M.; Uchiki, H.; Murakami, K.; Miyachi, H. Design, Synthesis and Evaluation of Substituted Phenylpropanoic Acid Derivatives as Human Peroxisome Proliferator-Activated Receptor Activators; Discovery of Potent and Human PPAR α Subtype-Selective Activators. *J. Med. Chem.* **2003**, *46*, 3581–3599. [[CrossRef](#)]
15. Oyama, T.; Kamata, S.; Ishii, I.; Miyachi, H. Crystal structures of the human peroxisome proliferator-activated receptor (PPAR) α ligand-binding domain in complexes with a series of phenylpropanoic acid derivatives generated by a ligand-exchange soaking method. *Bio. Pharm. Bull.* **2021**. Accepted for publication.
16. Kasuga, J.; Yamasaki, D.; Araya, Y.; Nakagawa, A.; Makishima, M.; Doi, T.; Hashimoto, Y.; Miyachi, H. Design, synthesis and evaluation of a novel series of α -substituted phenylpropanoic acid derivatives as human peroxisome proliferator-activated receptor (PPAR) α/δ dual agonists for the treatment of metabolic syndrome. *Bioorg. Med. Chem.* **2006**, *14*, 8405–8414. [[CrossRef](#)] [[PubMed](#)]
17. Araya, Y.; Kasuga, J.; Toyota, K.; Hirakawa, Y.; Oyama, T.; Makishima, M.; Morikawa, K.; Hashimoto, Y.; Miyachi, H. Structure-Based Design and Synthesis of Fluorescent PPAR α/δ Co-agonist and Its Application as a Probe for Fluorescent Polarization Assay of PPAR δ Ligands. *Chem. Pharm. Bull.* **2008**, *56*, 1357–1359. [[CrossRef](#)] [[PubMed](#)]
18. Kasuga, J.; Nakagome, I.; Aoyama, A.; Sako, K.; Ishizawa, M.; Ogura, M.; Makishima, M.; Hirono, S.; Hashimoto, Y.; Miyachi, H. Design, synthesis, and evaluation of potent, structurally novel peroxisome proliferator-activated receptor (PPAR) δ -selective agonists. *Bioorg. Med. Chem.* **2007**, *15*, 5177–5190. [[CrossRef](#)] [[PubMed](#)]
19. Kasuga, J.; Yamasaki, D.; Ogura, K.; Shimizu, M.; Sato, M.; Makishima, M.; Doi, T.; Hashimoto, Y.; Miyachi, H. SAR-oriented discovery of peroxisome proliferator-activated receptor pan agonist with a 4-adamantylphenyl group as a hydrophobic tail. *Bioorg. Med. Chem. Lett.* **2008**, *18*, 1110–1115. [[CrossRef](#)] [[PubMed](#)]
20. Ohashi, M.; Oyama, T.; Nakagome, I.; Satoh, M.; Nishio, Y.; Nobusada, H.; Hirono, S.; Morikawa, K.; Hashimoto, Y.; Miyachi, H. Design, Synthesis, and Structural Analysis of Phenylpropanoic Acid-Type PPAR γ -Selective Agonists: Discovery of Reversed Stereochemistry-Activity Relationship. *J. Med. Chem.* **2011**, *54*, 331–341. [[CrossRef](#)]
21. Ohashi, M.; Oyama, T.; Putranto, E.W.; Waku, T.; Nobusada, H.; Kataoka, K.; Matsuno, K.; Yashiro, M.; Morikawa, K.; Huh, N.H.; et al. Design and synthesis of a series of α -benzyl phenylpropanoic acid-type peroxisome proliferator-activated receptor (PPAR) γ partial agonists with improved aqueous solubility. *Bioorg. Med. Chem.* **2013**, *21*, 2319–2332. [[CrossRef](#)]
22. Ohashi, M.; Oyama, T.; Miyachi, H. Different structures of the two peroxisome proliferator-activated receptor γ (PPAR γ) ligand-binding domains in homodimeric complex with partial agonist, but not full agonist. *Bioorg. Med. Chem. Lett.* **2015**, *25*, 2639–2644. [[CrossRef](#)]
23. Oyama, T.; Toyota, K.; Waku, T.; Hirakawa, Y.; Nagasawa, N.; Kasuga, J.; Hashimoto, Y.; Miyachi, H.; Morikawa, K. Adaptability and selectivity of human peroxisome proliferator-activated receptor (PPAR) pan agonists revealed from crystal structures. *Acta Crystallogr. D Biol. Crystallogr.* **2009**, *65*, 786–795. [[CrossRef](#)]
24. Kuwabara, N.; Oyama, T.; Tomioka, D.; Ohashi, M.; Yanagisawa, J.; Shimizu, T.; Miyachi, H. Peroxisome proliferator-activated receptors (PPARs) have multiple binding points that accommodate ligands in various conformations: Phenylpropanoic acid-type PPAR ligands bind to PPAR in different conformations, depending on the subtype. *J. Med. Chem.* **2012**, *55*, 893–902. [[CrossRef](#)]
25. Ohashi, M.; Gamo, K.; Oyama, T.; Miyachi, H. Peroxisome proliferator-activated receptor γ (PPAR γ) has multiple binding points that accommodate ligands in various conformations: Structurally similar PPAR γ partial agonists bind to PPAR γ LBD in different conformations. *Bioorg. Med. Chem. Lett.* **2015**, *25*, 2758–2762. [[CrossRef](#)] [[PubMed](#)]
26. Evans, D.A.; Ennis, M.D.; Mathre, D.J. Asymmetric alkylation reaction of chiral imide enolates. A practical approach to the enantioselective synthesis of R-substituted carboxylic acid derivatives. *J. Am. Chem. Soc.* **1982**, *104*, 1737–1739. [[CrossRef](#)]

27. Daniel, D.; Andrew, A.S. Reductive N-alkylation of amides, carbamates and ureas. *Tetrahedron Lett.* **1999**, *40*, 2295–2298.
28. Murakami, K.; Tobe, K.; Ide, T.; Mochizuki, T.; Ohashi, M.; Akanuma, Y.; Yazaki, Y.; Kadowaki, T. A novel insulin sensitizer acts as a coligand for peroxisome proliferator activated receptor- α (PPAR- α) and PPAR- γ : Effect of PPAR- α activation on abnormal lipid metabolism in liver of Zucker fatty rats. *Diabetes* **1998**, *47*, 1841–1847. [[CrossRef](#)]
29. Nomura, M.; Kinoshita, S.; Satoh, H.; Maeda, T.; Murakami, K.; Tsunoda, M.; Miyachi, H.; Awano, K. (3-substituted benzyl)thiazolidine-2, 4-diones as structurally new antihyperglycemic agents. *Bioorg. Med. Chem. Lett.* **1999**, *9*, 533–538. [[CrossRef](#)]
30. Yajima, K.; Hirose, H.; Fujita, H.; Seto, Y.; Fujita, H.; Ukeda, K.; Miyashita, K.; Kawai, T.; Yamamoto, Y.; Ogawa, T.; et al. Combination therapy with PPAR γ and PPAR α agonists increases glucose-stimulated insulin secretion in db/db mice. *Am. J. Physiol.* **2003**, *284*, E966–E971.
31. Nomura, M.; Tanase, T.; Miyachi, H. Efficient asymmetric synthesis of (S)-2-ethylphenylpropanoic acid derivative, a selective agonist for human peroxisome proliferator-activated receptor α . *Bioorg. Med. Chem. Lett.* **2002**, *12*, 2101–2104. [[CrossRef](#)]
32. Miyachi, H.; Nomura, M.; Tanase, M.; Suzuki, M.; Murakami, K.; Awano, K. Enantio-dependent binding and transactivation of optically active phenylpropanoic acid derivatives at human peroxisome proliferator-activated receptor α . *Bioorg. Med. Chem. Lett.* **2002**, *12*, 333–335. [[CrossRef](#)]
33. Miyachi, H.; Nomura, M.; Tanase, T.; Takahashi, Y.; Ide, T.; Tsunoda, M.; Murakami, K.; Awano, K. Design, synthesis and evaluation of substituted phenylpropanoic acid derivatives as peroxisome proliferator-activated receptor (PPAR) activators: Novel human PPAR α -selective activators. *Bioorg. Med. Chem. Lett.* **2002**, *12*, 77–80. [[CrossRef](#)]
34. Miyachi, H.; Uchiki, H. Analysis of the critical structural determinant(s) of species-selective peroxisome proliferator-activated receptor α (PPAR α)-activation by phenylpropanoic acid-type PPAR α agonists. *Bioorg. Med. Chem. Lett.* **2003**, *13*, 3145–3149. [[CrossRef](#)]
35. Kamata, S.; Oyama, T.; Ishii, I. Preparation of co-crystals of human PPAR α -LBD and ligand for high-resolution X-ray crystallography. *STAR Protoc.* **2021**, *2*, 100364. [[CrossRef](#)] [[PubMed](#)]
36. Takayama, F.; Egashira, T.; Kawasaki, H.; Mankura, M.; Nakamoto, K.; Okada, S.; Mori, A. A Novel Animal Model of Nonalcoholic Steatohepatitis (NASH): Hypoxemia Enhances the Development of NASH. *J. Clin. Biochem. Nutr.* **2009**, *45*, 335–340. [[CrossRef](#)] [[PubMed](#)]
37. Nakamoto, K.; Takayama, F.; Mankura, M.; Hidaka, Y.; Egashira, T.; Ogino, T.; Kawasaki, H.; Mori, A. Beneficial Effects of Fermented Green Tea Extract in a Rat Model of Non-alcoholic Steatohepatitis. *J. Clin. Biochem. Nutr.* **2009**, *44*, 239–246. [[CrossRef](#)] [[PubMed](#)]
38. Day, C.D.; James, O.F.W. Steatohepatitis: A tale of two “hits”? *Gastroenterology* **1998**, *114*, 842–845. [[CrossRef](#)]
39. Tokushige, K.; Takakura, M.; Tsuchiya-Matsushita, N.; Taniai, M.; Hashimoto, E.; Shiratori, K. Influence of TNF gene polymorphism in Japanese patients with NASH and simple steatosis. *J. Hepatol.* **2007**, *46*, 1104–1110. [[CrossRef](#)]
40. Burt, A.D.; Mutton, A.; Day, C.P. Diagnosis and interpretation of steatosis and steatohepatitis. *Semin. Diagn. Pathol.* **1998**, *15*, 246–258.
41. Holoman, J.; Glasa, J.; Galbavy, S.; Danis, D.; Molnarova, A.; Kazar, J.; Bednarova, A.; Misianik, J. Serum markers of liver fibrogenesis, and liver histology findings in patients with chronic liver diseases. *Bratisl. Lek. Listy.* **2002**, *103*, 70–75. [[PubMed](#)]
42. Masaro, C.; Acosta, E.; Ortiz, J.A.; Marrero, P.F.; Hegardt, F.G.; Haro, D. Control of Human Muscle-type Carnitine Palmitoyltransferase I Gene Transcription by Peroxisome Proliferator-activated Receptor. *J. Biol. Chem.* **1998**, *273*, 8560–8563. [[CrossRef](#)]
43. Mandard, S.; Zandbergen, F.; Tan, N.S.; Escher, P.; Patsouris, D.; Koenig, W.; Kleemann, R.; Bakker, A.; Veenman, F.; Wahli, W.; et al. The direct peroxisome proliferator-activated receptor target fasting-induced adipose factor (FIAF/PGAR/ANGPTL4) is present in blood plasma as a truncated protein that is increased by fenofibrate treatment. *J. Biol. Chem.* **2004**, *279*, 34411–34420. [[CrossRef](#)]
44. Bassene, C.E.; Suzenet, F.; Hennuyer, N.; Staels, B.; Caignard, D.H.; Dacquet, C.; Renard, P.; Guillaumet, G. Studies towards the conception of new selective PPAR β/δ ligands. *Bioorg. Med. Chem. Lett.* **2006**, *16*, 4528–4532. [[CrossRef](#)] [[PubMed](#)]
45. Weigand, S.; Bischoff, H.; Dittrich-Wengenroth, E.; Heckroth, H.; Lang, D.; Vaupel, A.; Woltering, M. Minor structural modifications convert a selective PPAR α agonist into a potent, highly selective PPAR δ agonist. *Bioorg. Med. Chem. Lett.* **2005**, *15*, 4619–4623. [[CrossRef](#)]
46. Epple, R.; Azimioara, M.; Russo, R.; Bursulaya, B.; Tian, S.S.; Gerken, A.; Iskandar, M. 1,3,5-trisubstituted aryls as highly selective PPAR δ agonists. *Bioorg. Med. Chem. Lett.* **2006**, *16*, 2969–2973. [[CrossRef](#)]
47. Epple, R.; Azimioara, M.; Russo, R.; Xie, Y.; Wang, X.; Cow, C.; Wityak, J.; Karanewsky, D.; Bursulaya, B.; Kreuzsch, A.; et al. 3,4,5-trisubstituted isoxazoles as novel PPAR δ agonists: Part 2. *Bioorg. Med. Chem. Lett.* **2006**, *16*, 5488–5492. [[CrossRef](#)] [[PubMed](#)]
48. Epple, R.; Russo, R.; Azimioara, M.; Cow, C.; Xie, Y.; Wang, X.; Wityak, J.; Karanewsky, D.; Gerken, A.; Iskandar, M.; et al. 3,4,5-trisubstituted isoxazoles as novel PPAR δ agonists: Part 1. *Bioorg. Med. Chem. Lett.* **2006**, *16*, 4376–4380. [[CrossRef](#)]
49. Xu, H.E.; Lambert, M.H.; Montana, V.G.; Parks, D.J.; Blanchard, S.G.; Brown, P.J.; Sternbach, D.D.; Lehmann, J.M.; Wisely, G.B.; Willson, T.M.; et al. Molecular recognition of fatty acids by peroxisome proliferator-activated receptors. *Mol. Cell* **1999**, *3*, 397–403. [[CrossRef](#)]
50. Smith, D.S.; Eremin, S.A. Fluorescence polarization immunoassays and related methods for simple, high-throughput screening of small molecules. *Anal. Bioanal. Chem.* **2008**, *391*, 1499–1507. [[CrossRef](#)] [[PubMed](#)]
51. Royer, C.A. Probing protein folding and conformational transitions with fluorescence. *Chem. Rev.* **2006**, *106*, 1769–1784. [[CrossRef](#)]

52. Fruchart, J.C.; Staels, B.; Duriez, P. The role of fibric acids in atherosclerosis. *Curr. Atheroscler. Rep.* **2001**, *3*, 83–92. [[CrossRef](#)] [[PubMed](#)]
53. Yamaguchi, K.; Lee, S.H.; Eling, T.E.; Baek, S.J. A novel peroxisome proliferator-activated receptor γ ligand, MCC-555, induces apoptosis via posttranscriptional regulation of NAG-1 in colorectal cancer cells. *Mol. Cancer Ther.* **2006**, *5*, 1352–1361. [[CrossRef](#)]
54. Ambele, M.A.; Dhanraj, P.; Giles, R.; Pepper, M.S. Adipogenesis: A Complex Interplay of Multiple Molecular Determinants and Pathways. *Int. J. Mol. Sci.* **2020**, *21*, 4283. [[CrossRef](#)] [[PubMed](#)]
55. Zandbergen, F.; Mandard, S.; Escher, P.; Tan, N.S.; Patsouris, D.; Jatko, T.; Rojas-Caro, S.; Madore, S.; Wahli, W.; Tafuri, S.; et al. The G₀/G₁ switch gene 2 is a novel PPAR target gene. *Biochem. J.* **2005**, *392*, 313–324. [[CrossRef](#)]
56. Tachibana, K.; Kobayashi, Y.; Tanaka, T.; Tagami, M.; Sugiyama, A.; Katayama, T.; Ueda, C.; Yamasaki, D.; Ishimoto, K.; Sumitomo, M.; et al. Gene expression profiling of potential peroxisome proliferator-activated receptor (PPAR) target genes in human hepatoblastoma cell lines inducibly expressing different PPAR isoforms. *Nucl. Recept.* **2005**, *3*, 3. [[CrossRef](#)] [[PubMed](#)]
57. Hong, J.; Samudio, I.; Liu, S.; Abdelrahim, M.; Safe, S. Peroxisome Proliferator-Activated Receptor-Dependent Activation of p21 in Panc-28 Pancreatic Cancer Cells Involves Sp1 and Sp4 Proteins. *Endocrinology* **2004**, *145*, 5774–5785. [[CrossRef](#)]
58. Ming, M.; Yu, J.P.; Meng, X.Z.; Zhou, Y.H.; Yu, H.G.; Luo, H.S. Effect of ligand troglitazone on peroxisome proliferator-activated receptor γ expression and cellular growth in human colon cancer cells. *World J. Gastroenterol.* **2006**, *7*, 7263–7270. [[CrossRef](#)]
59. Kasuga, J.; Ishikawa, M.; Yonehara, M.; Makishima, M.; Hashimoto, Y.; Miyachi, H. Improvement of water-solubility of biarylcarboxylic acid peroxisome proliferator-activated receptor (PPAR) δ -selective partial agonists by disruption of molecular planarity/symmetry. *Bioorg. Med. Chem.* **2010**, *18*, 7164–7173. [[CrossRef](#)]
60. Yashiro, M.; Chung, Y.S.; Nishimura, S.; Inoue, T.; Sowa, M. Peritoneal metastatic models for human scirrhous gastric carcinoma in nude mice. *Clin. Exp. Metastasis* **1996**, *14*, 43–54. [[CrossRef](#)]
61. Takahashi, N.; Okumura, T.; Motomura, W.; Fujimoto, Y.; Kawabata, I.; Kohgo, Y. Activation of PPAR γ inhibits cell growth and induces apoptosis in human gastric cancer cells. *FEBS Lett.* **1999**, *455*, 135–139. [[CrossRef](#)]
62. Cheon, C.W.; Kim, D.H.; Cho, Y.H.; Kim, J.H. Effects of ciglitazone and troglitazone on the proliferation of human stomach cancer cells. *World J. Gastroenterol.* **2009**, *15*, 310–320. [[CrossRef](#)]
63. Leo, C.; Yang, X.; Liu, J.; Li, H.; Chen, J.D. Role of Retinoid Receptor Coactivator Pockets in Cofactor Recruitment and Transcriptional Regulation. *J. Biol. Chem.* **2001**, *276*, 23127–23134. [[CrossRef](#)] [[PubMed](#)]
64. Benko, S.; Love, J.D.; Beládi, M.; Schwabe, J.W.; Nagy, L. Molecular Determinants of the Balance between Co-repressor and Co-activator Recruitment to the Retinoic Acid Receptor. *J. Biol. Chem.* **2003**, *278*, 43797–43806. [[CrossRef](#)]
65. Yamagishi, K.; Yamamoto, K.; Mochizuki, Y.; Nakano, T.; Yamada, S.; Tokiwa, H. Flexible ligand recognition of peroxisome proliferator-activated receptor- γ (PPAR γ). *Bioorg. Med. Chem. Lett.* **2010**, *20*, 3344–3347. [[CrossRef](#)]
66. Pochetti, G.; Godio, C.; Mitro, N.; Caruso, D.; Galmozzi, A.; Scurati, S.; Loidis, F.; Fratiolla, G.; Tortollera, P.; Laghezza, A.; et al. Insights into the mechanism of partial agonism: Crystal structures of the peroxisome proliferator-activated receptor γ ligand-binding domain in the complex with two enantiomeric ligands. *J. Biol. Chem.* **2007**, *282*, 17314–17324. [[CrossRef](#)] [[PubMed](#)]
67. Carbonara, G.; Di Giovanni, C.; Fracchiolla, G.; Laghezza, A.; Lavecchia, A.; Loidice, F.; Montanari, R.; Novellino, E.; Parente, M.; Piemontese, L.; et al. Synthesis, biological evaluation and molecular investigation of fluorinated peroxisome proliferator-activated receptors α/γ dual agonists. *Bioorg. Med. Chem.* **2012**, *20*, 2141–2151.
68. Blanchard, S.G.; Cobb, J.E.; Collins, J.L.; Cooper, J.P.; Goreham, D.M.; Holmes, C.P.; Hull-Ryde, E.A.; Kliewer, S.A.; Lehmann, J.M.; Lenhard, J.M.; et al. Peroxisome proliferator-activated receptor γ ligand inhibits adipocyte differentiation. *Proc. Natl. Acad. Sci. USA* **1999**, *96*, 6102–6106.
69. Chao, Y.S.; Chen, C.T.; Chen, H.Y.; Chen, X.; Goparaju, C.M.; Hsieh, H.P.; Hsu, J.T.; Huang, C.F.; Lee, H.J.; Liao, C.C.; et al. Structure-Based Drug Design of a Novel Family of PPAR γ Partial Agonists: Virtual Screening, X-ray Crystallography, and in Vitro/in Vivo Biological Activities. *J. Med. Chem.* **2006**, *49*, 2703–2712.
70. Abdalla, D.S.; Amato, A.A.; Ayers, S.D.; Baxter, J.D.; Brennan, R.G.; Carvalho, B.M.; Figueira, A.C.; Galdino, S.L.; Lima, M.C.; Lin, J.Z.; et al. GQ-16, a novel peroxisome proliferator-activated receptor (PPAR γ) ligand, promotes insulin sensitization without weight gain. *J. Biol. Chem.* **2012**, *287*, 28169–28179.
71. Kawai, M.; Rosen, C.J. PPAR γ : A circadian transcription factor in adipogenesis and osteogenesis. *Nat. Rev. Endocrinol.* **2010**, *6*, 629–636. [[CrossRef](#)]
72. Taygerly, J.P.; McGee, L.R.; Rubenstein, S.M.; Houze, J.B.; Cushing, T.D.; Li, Y.; Motani, A.; Chen, J.L.; Frankmoelle, W.; Ye, G.; et al. Discovery of INT131: A selective PPAR γ modulator that enhances insulin sensitivity. *Bioorg. Med. Chem.* **2013**, *21*, 979–992. [[CrossRef](#)]
73. Lu, W.; Lau, F.; Liu, K.; Wood, H.B.; Zhou, G.; Chen, Y.; Li, Y.; Akiyama, T.E.; Castriota, G.; Einstein, M.; et al. Benzimidazolones: A New Class of Selective Peroxisome Proliferator-Activated Receptor γ (PPAR γ) Modulators. *J. Med. Chem.* **2011**, *54*, 8541–8554. [[CrossRef](#)]
74. Bruning, J.B.; Chalmers, M.J.; Prasad, S.; Busby, S.A.; Kamenecka, T.M.; He, Y.; Nettles, K.W.; Griffin, P.R. Partial Agonists Activate PPAR γ Using a Helix 12 Independent Mechanism. *Structure* **2007**, *15*, 1258–1271. [[CrossRef](#)] [[PubMed](#)]
75. Hosoda, S.; Tanatani, A.; Wakabayashi, K.; Makishima, M.; Imai, K.; Miyachi, H.; Nagasawa, K.; Hashimoto, Y. Ligands with a 3,3-diphenylpentane skeleton for nuclear vitamin D and androgen receptors: Dual activities and metabolic activation. *Bioorg. Med. Chem.* **2006**, *14*, 5489–5502. [[CrossRef](#)]

76. Asano, L.; Ito, I.; Kuwabara, N.; Waku, T.; Yanagisawa, J.; Miyachi, H.; Shimizu, T. Structural basis for vitamin D receptor agonism by novel non-secosteroidal ligands. *FEBS Lett.* **2013**, *587*, 957–963. [[CrossRef](#)]
77. Kainuma, M.; Makishima, M.; Hashimoto, Y.; Miyachi, H. Design, synthesis, and evaluation of non-steroidal farnesoid X receptor (FXR) antagonist. *Bioorg. Med. Chem.* **2007**, *15*, 2587–2600. [[CrossRef](#)] [[PubMed](#)]
78. Kainuma, M.; Kasuga, J.; Hosoda, S.; Wakabayashi, K.; Tanatani, A.; Nagasawa, K.; Miyachi, H.; Makishima, M.; Hashimoto, Y. Diphenylmethane skeleton as a multi-template for nuclear receptor ligands: Preparation of FXR and PPAR ligands. *Bioorg. Med. Chem. Lett.* **2006**, *16*, 3213–3218. [[CrossRef](#)]
79. Kasuga, J.; Ishida, S.; Yamasaki, D.; Makishima, M.; Doi, T.; Hashimoto, Y.; Miyachi, H. Novel biphenylcarboxylic acid peroxisome proliferator-activated receptor (PPAR) α selective antagonists. *Bioorg. Med. Chem. Lett.* **2009**, *19*, 6595–6599. [[CrossRef](#)] [[PubMed](#)]
80. Ohashi, M.; Gamo, K.; Tanaka, Y.; Waki, M.; Beniyama, Y.; Matsuno, K.; Wada, J.; Tenta, M.; Eguchi, J.; Makishima, M.; et al. Structural design and synthesis of arylalkynyl amide-type peroxisome proliferator-activated receptor γ (PPAR γ)-selective antagonists based on the helix12-folding inhibition hypothesis. *Eur. J. Med. Chem.* **2015**, *27*, 53–67. [[CrossRef](#)]
81. Aoyama, A.; Aoyama, H.; Dodo, K.; Makishima, M.; Hashimoto, Y.; Miyachi, H. LXR Antagonists with a 5-Substituted Phenanthridin-6-one Skeleton: Synthesis and LXR Transrepression Activities of Conformationally Restricted Carba-T0901317 Analogs. *Heterocycles* **2008**, *76*, 137–142. [[CrossRef](#)]
82. Kishida, K.; Aoyama, A.; Hashimoto, Y.; Miyachi, H. Design and synthesis of phthalimide-based fluorescent LXR antagonists. *Chem. Pharm. Bull.* **2010**, *58*, 1525–1528. [[CrossRef](#)] [[PubMed](#)]
83. Nakagawa, A.; Uno, S.; Makishima, M.; Miyachi, H.; Hashimoto, Y. Progesterone receptor antagonists with a 3-phenylquinazoline-2,4-dione/2-phenylisoquinoline-1,3-dione skeleton. *Bioorg. Med. Chem.* **2008**, *16*, 7046–7054. [[CrossRef](#)] [[PubMed](#)]